

FLUID MODELING OF EXHAUST GAS DISPERSION
FOR THE UNIVERSITY OF COLORADO
SCHOOL OF PHARMACY

Prepared by

Douglas K. Parce*

Robert N. Meroney⁺

Final Report

for

Physical Plant and Maintenance Department

University of Colorado Health Sciences Center

Denver, Colorado 80262

* Graduate Research Assistant

⁺ Professor, Civil Engineering

FLUID MECHANICS AND WIND ENGINEERING PROGRAM



CSU Contract No. 2-98220

CER90-91DKP-RNM-8

**FLUID MODELING OF EXHAUST GAS DISPERSION
FOR THE UNIVERSITY OF COLORADO
SCHOOL OF PHARMACY**

Final Report
(July 1990 - November 1990)

Prepared by

Douglas K. Parce*
Robert N. Meroney+

for

Physical Plant and Maintenance Department
University of Colorado Health Sciences Center
Denver, Colorado 80262

* Graduate Research Assistant
+ Professor, Civil Engineering
FLUID MECHANICS AND WIND ENGINEERING PROGRAM



Colorado
State
University

CSU Contract No. 2-98220
CER90-91DKP-RNM-8

ABSTRACT

A wind-tunnel study was conducted in the Fluid Dynamics and Diffusion Laboratory at Colorado State University on a model of a planned addition to the University of Colorado Health Sciences Center (UCHSC). A 1:150 scale model of the new building, the School of Pharmacy (SOP) was added to an existing model of the UCHSC. It was used to collect information about the behavior of exhaust plumes and the probability of exhaust reentrainment into the new addition. Results are given in terms of normalized concentrations (K coefficients) to permit concentration estimates for alternative traffic, exhaust and wind speed combinations; but the decision as to the preferred configuration must be made with regard to current air-quality standards and building esthetics.

TABLE OF CONTENTS

Abstract	i
List of Figures	iii
List of Tables	iv
List of Symbols	v
1 Introduction	1
2 School of Pharmacy Study Summary	2
3 Model Design and Construction	3
4 Data Acquisition and Analysis Techniques	4
4.1 Wind Tunnel Facilities	4
4.2 Wind Profile Measurements	4
4.2.1 Single-Hot-Film Probe Measurements	5
4.2.2 Velocity Standard	5
4.2.3 Error Statement	5
4.3 Flow Visualization Techniques	6
4.4 Concentration Measurement Techniques	6
4.4.1 Gas Chromatograph & Integrator	6
4.4.2 Sampling System	7
4.4.3 Concentration Test Procedure	7
4.4.4 Error Statement	8
5 Visualization Study Results	9
6 Concentration Study Results	11
7 Discussion and Recommendations	12
Figures	13
Tables	26
References	36
Appendix: Fluid Modeling	39
A.1 Dimensionless Parameters	39
A.1.1 The Reynolds Number	41
A.1.2 The Richardson Number	41
A.2 Performance of Previous Fluid Modeling Performance	42
A.3 Modeling of Bluff Bodies	44
A.3.1 Simulation Criteria	44
A.3.2 Obstacle size & detail	45
A.3.3 Upstream Fetch Modeling	45
A.3.4 Blockage Effects	46
A.3.5 Flow over Sharp-Edged Obstacles	46
A.3.6 Flow over Rounded Obstacles	48
A.4 Modeling of Plume Motion	49

LIST OF FIGURES

Figure 1	Map of University Hospital Health Sciences Center . . .	14
Figure 2	Environmental Wind Tunnel	15
Figure 3	Trace Gas Release and Sampling Schematic	15
Figure 4	Low Wind Speed Velocity Profile	16
Figure 5	Low Wind Speed Turbulence Profile	16
Figure 6	Medium Wind Speed Velocity Profile	17
Figure 7	Medium Wind Speed Turbulence Profile	17
Figure 8	High Wind Speed Velocity Profile	18
Figure 9	High Wind Speed Turbulence Profile	18
Figure 10	Layout of Concentration Sampling Points	19
Figure 11	SOP Intake Vent Cross-Contamination (East End)	20
Figure 12	SOP Intake Vent Cross-Contamination (West End)	20
Figure 13	SOM Intake Vent Cross-Contamination (Large well)	21
Figure 14	Exhaust Contamination near SOP main entrance	21
Figure 15	Concentrations for a Low Speed, North Wind	22
Figure 16	Concentrations for a Low Speed, North-East Wind	22
Figure 17	Concentrations for a Low Speed, South-East Wind	23
Figure 18	Concentrations for a Low Speed, South-West Wind	23
Figure 19	Concentrations for a High Speed, North Wind	24
Figure 20	Concentrations for a High Speed, North-East Wind	24
Figure 21	Concentrations for a High Speed, South-East Wind	25
Figure 22	Concentrations for a High Speed, South-West Wind	25

LIST OF TABLES

Table 1	Velocity and Turbulence Profile Data (Low Wind Speed)	. . 27
Table 2	Velocity and Turbulence Profile Data (Medium Wind Speed)	. 28
Table 3	Velocity and Turbulence Profile Data (High Wind Speed)	. . 29
Table 4	Visualization Test Plan 30
Table 5	Concentration Test Plan 31
Table 6	Run 1 Concentration Test Data 32
Table 6	Run 2 Concentration Test Data 32
Table 7	Run 3 Concentration Test Data 33
Table 7	Run 4 Concentration Test Data 33
Table 8	Run 5 Concentration Test Data 34
Table 8	Run 6 Concentration Test Data 34
Table 9	Run 7 Concentration Test Data 35
Table 9	Run 8 Concentration Test Data 35

LIST OF SYMBOLS

A, B, C	Constants
BR	Blockage ratio
C_f	Friction Coefficient
C_p	Specific heat capacity at constant pressure
E	Voltage
g	Gravitational acceleration (9.81 m s^{-2})
h	Height of the obstacle
K	Normalized concentration coefficient
k	Roughness length
L	Length
Q	Flow rate
S	Distance downwind of the obstacle
T	Temperature
U	Wind velocity
u_*	Friction velocity
X	Distance (East - West)
Y	Distance (North - South)
Z	Height above ground (relative to some elevation reference)
z_o	Roughness length

Greek Characters

δ	Boundary layer thickness
Δ	Change in...
κ	Thermal conductivity
Γ	Actual adiabatic lapse rate
Γ_d	Dry Adiabatic Lapse Rate
μ	Dynamic viscosity
ν	Kinematic viscosity
ρ	Density
σ	Shear stress
χ	Concentration ratio
Ω	Angular velocity of earth - $0.726 \times 10^{-4} \text{ rad/s}$

Dimensionless Parameters

Ec	Eckert number
Fr	Froude number
Ma	Mach number
Re	Reynolds number
Ri	Bulk Richardson number
Ro	Rossby number
Pr	Prandtl number
V	Volume flux ratio ($Q/U_H L^2$)
We	Weber number

Abbreviations

ABL	Atmospheric Boundary Layer
BRC	Bimedical Research Center
calib	calibration
CSU	Colorado State University
EWT	Environmental Wind Tunnel
FDDL	Fluid Dynamics and Diffusion Laboratory
FID	Flame Ionization Detector
GC	Gas Chromatograph
SOM	School of Medicine
SOP	School of Pharmacy
TSI	Thermo-System, Inc.
UCHSC	University of Colorado Health Sciences Center

Subscripts

a	Air, Ambient
bg	Background
g	Gas (trace/source gas)
m	Model (model-scale)
mea	Measured
p	Prototype (full-scale)
s	Source
1	First
2	Second

1 INTRODUCTION

In anticipation of the addition of the proposed School of Pharmacy (SOP) to the University of Colorado's Health Sciences Center (UCHSC) the designers should have a detailed understanding of the complex aerodynamics of exhaust plumes emitted from the SOP as well as from surrounding structures. This knowledge, coupled with information about the SOP's ventilation intakes will be useful in creating a design which minimizes the probability of exhaust-intake cross-contamination for the new building.

Tan and Meroney (1989) previously conducted a study with regard to exhaust gas dispersion about the UCHSC campus. The model used in this analysis was originally constructed for use during the earlier study. Tan and Meroney evaluated the influence that the Biomedical Research Center addition would have on plume aerodynamics over the UCHSC campus. This study considers the influence of the SOP addition on ventilator entrainment.

The scaled model of the UCHSC with the SOP addition was placed in the Environmental Wind Tunnel (EWT) in the Fluid Dynamics and Diffusion Laboratories (FDDL) at Colorado State University (CSU). Wind tunnels simulate the earth's atmospheric boundary layer (ABL) which is the primary meteorological region in which localized pollution dispersion occurs. Individual experiments or "test runs" were conducted in groups as follows:

Visualizations

- Group 1A Eight wind directions, Low wind speed (5 mph)
- Group 2A Eight wind directions, Medium wind speed (10 mph)
- Group 3A Eight wind directions, High wind speed (15 mph)

Concentrations

- Group 1B Four selected wind directions, Low wind speed
- Group 2B Four selected wind directions, High wind speed

2 SCHOOL OF PHARMACY STUDY SUMMARY

A physical modeling study of the UCHSC vent buildings was performed to assist in predicting environmental impacts for several proposed stack-building configurations. This involved:

- 1) Construction at 1:150 reduced scale of all buildings within 800 feet of the School of Pharmacy site,
- 2) Incorporation of this model into a wind tunnel facility with the appropriate upwind roughness for this site,
- 3) Acquisition of velocity and turbulence profiles for the modeled site,
- 4) Video taping of three different model plumes for 8 different wind directions, and
- 5) Measurement of concentrations at 48 different sampling locations for two wind speeds and four wind directions.

Since the previous study by Tan and Meroney (1989) covered in some detail the modeling parameters and conventions used in this study, further discussion is not offered here. A summary of fluid modeling pertinent to this study may be found in the appendix.

3 MODEL DESIGN AND CONSTRUCTION

The wind approaches the Denver city over suburban roughness. Replicas (at reduced scale of 1:150) of all buildings within 800 feet of the School of Pharmacy were constructed and placed on the downwind turntable in the wind tunnel. The wind characteristics approaching the UCHSC center site were simulated with spires at the tunnel entrance and thirty feet of generic suburban roughness (constructed from one-inch foam cubes) upwind of the model.

The modeling parameter decision process yielded the following conclusions:

1. The maximum field dispersion distance of interest and size of the FDDL EWT resulted in the selection of a 1:150 model length scale ratio.
2. Wind-tunnel floor roughness was incorporated to produce properly scaled wind shear and turbulent structure.
3. Model wind speed and stack exit velocity were set at large enough magnitudes to assure Reynolds number independence of approach flow and stack flow.
4. Model wind velocity to plume velocity ratios were set equal to the field values; thus assuring similarity of plume trajectories.

In the previous study by Tan and Meroney (1989), for which the model was originally built, a model scale of 1:150 was selected. This decision was based on atmospheric data over the UCHSC area, the size of the desired concentration grid, and modeling constraints discussed in the appendix. Since the EWT (see figure 2) had a 12 foot turntable this allowed for the reduced scale construction of all significant buildings within a 800 foot radius of the SOP site. The location of the School of Pharmacy along with a circle denoting the portion of the Denver area which was replicated is shown in figure 1.

The buildings surrounding the vent structures were fabricated from styrofoam and were topped with masonite to improve the durability of the model. They were placed in their appropriate locations on a 12 foot diameter masonite sheet. The topography changes were modeled by layering the appropriate number of 1/4 inch masonite sheets to match the land contours within the modeled area. All roads were then painted on the platform for visual reference. The terrain upwind of the turntable area was modeled with a generic roughness. Health Science Center buildings (including the School of Pharmacy) were constructed from masonite and plexiglass to permit the incorporation of ventilator plenums and accurate placement of inlet and exhaust openings. The primary ventilator buildings in this study were the School of Pharmacy, Biomedical Research Center, and the School of Medicine Annex.

4 DATA ACQUISITION AND ANALYSIS TECHNIQUES

Laboratory measurement techniques are discussed in this section, along with conversion methods used to relate measured model quantities to their meaningful field equivalents. Some of the methods used are conventional and need little elaboration.

4.1 Wind Tunnel Facilities

The experiments were performed in the Environmental Wind Tunnel (EWT) shown in figure 2. This wind tunnel, especially designed to study atmospheric flow phenomena, incorporates special features such as an adjustable ceiling, a rotating turntable and a long test section to permit adequate reproduction of micrometeorological behavior. Mean wind speeds of 0.1 to 15 m/sec in the EWT can be obtained. Boundary-layer thickness up to 1.2 m can be developed "naturally" over the downstream 6 m of the EWT test section by using vortex generators at the test section entrance and surface roughness on the floor. The flexible test section on the EWT roof is adjustable in height to permit the longitudinal pressure gradient to be set at zero.

4.2 Wind Profile Measurements

Velocity measurements were made with a single-hot-film probe and anemometry equipment manufactured by Thermo-System, Inc. (TSI). The probe was traversed vertically through the simulated ABL, with the mean velocity and turbulence intensity at various elevations being transmitted to an IBM computer for later comparison to the ABL in the vicinity of the SOP. The site model was located on a turntable, thereby allowing different wind directions to be easily simulated.

Tables 1 through 3 present the data for the profiles. Figures 4 through 9 display plots of the mean velocity and longitudinal turbulent intensity profiles. The height coordinate in these tables and figures has been normalized by a model reference height of 1 meter (equivalent field height of 492 feet). To obtain actual field heights multiply the normalized value by 492. Since a neutral boundary layer's velocity is invariant with respect to wind speed the normalized profiles presented can be converted to any field velocity at a specific height by the appropriate multiplicative constant.

The approach mean velocity profile for a suburban roughness condition was regressed to find the best log-log and log-linear fit. The log-log regression ($U/U_r = (z/z_r)^p$) produced a power law exponent, p , equal to 0.36. The log-linear regression ($U/u_* = 2.5 \ln\{(z-d)/z_o\}$) found a best fit roughness length, z_o , of 0.79 meters (field scale) and a displacement thickness, d , of zero.

4.2.1 Single-Hot-Film Probe Measurements

Single-hot-film (TSI 1210 Sensor) measurements were used to document the longitudinal turbulence levels for the approach flow conditions. During calibration the probe voltages were recorded at several velocities covering the range of interest. These voltage-velocity (E,U) pairs were then regressed to the equation $E^2 = A + BU^c$ via a least squares approach for various assumed values of the exponent c. Convergence to the minimum residual error was accelerated by using the secant method to find the best new estimate for the exponent c.

The hot-film-probe was mounted on a vertical traverse and positioned over the measurement location in the wind tunnel. The anemometer's output voltage was digitized and stored within an IBM AT computer. This voltage time series was converted to a velocity time series using the inverse of the calibration equation; $U = [(E^2 - A)/B]^{1/c}$. The velocity time series was then analyzed for pertinent statistical quantities, such as mean velocity and root-mean-square turbulent velocity fluctuations. The computer system would move the velocity probe to a specified vertical position, acquire the data, and then move on to the next vertical position; thus obtaining an entire vertical velocity profile automatically.

4.2.2 Velocity Standard

The velocity standard used for the low wind speed consisted of a Matheson Model 8116-0154 mass flowmeter and a profile conditioning section designed and calibrated by the Fluid Dynamics and Diffusion (FDDL) staff at Colorado State University (CSU). The mass flowmeter measures mass flow rate independent of temperature and pressure. The profile conditioning section forms a flat velocity profile of very low turbulence at the position where the hot-film-probe is located. Incorporating a measurement of the ambient atmospheric pressure, temperature and a profile correction factor permits the calibration of velocity at the measurement station from 0.15-2.2 m/s to within ± 5 percent. The velocity standard used for the medium and high wind speeds included the use of a TSI model 1125 calibrator, and a Datametrix model 1018 electronic manometer. The manometer is used to measure the pressure differential across the 'nozzle' of the TSI calibrator. The calibrator produces a uniform velocity jet with low turbulence within which the hot-film-probe is suspended. This allows for similarly accurate calibration of the hot-film sensor at velocities greater than 1 m/s.

4.2.3 Error Statement

The calibration curve yielded hot film anemometer velocities that were always within 2 percent of the known calibrator velocity. Considering the accumulative effect of calibrator, calibration curve fit and other errors, the model velocity time series should be regarded as accurate to within 10 percent.

4.3 Flow Visualization Techniques

A visible plume was produced by mixing the metered simulant gas with smoke produced by a smoke generator, (Rosco Fog/Smoke Machine model 1200) and then out of the modeled stack. The visible plumes for each test were recorded on S-VHS video cassettes with a Panasonic Professional/Industrial camera/recorder system (AG-450). Run number titles were placed on the video cassette with a title generator.

A total of twenty-four visualization test runs were recorded for the School of Pharmacy. The equivalent prototype wind velocity for the first eight tests (1-8) were at 2.2 m/s (5 mph), the next eight tests (9-16) were at 4.5 m/s (10 mph), and the last eight tests (17-24) were at 6.7 m/s (15 mph); all taken at an equivalent height of 10 meters (32.8 ft).

Documentation on video cassette of all visual tests have been provided to the sponsor prior to this report. Given a model to field wind speed ratio of 1:2 and a model to field length scale ratio of 1:150, the time scale ratio between the model and the field is 1:75. Thus phenomena observed over the model in the wind tunnel will occur 75 times faster than observed at full scale. So the plume motion which occurs over a one minute time period on the S-VHS tape would require one-hour and fifteen minutes to occur at full scale.

4.4 Concentration Measurement Techniques

The experimental measurements of concentration were performed using a Hewlett Packard gas-chromatograph, integrator and sampling system designed by FDDL staff. By maintaining flow similarity between model and field conditions, relative concentrations (χ/Q) for a given source configuration, building configuration and wind direction will be invariant. The wind tunnel relative concentration measurements for the UCHSC building complex will be the same as those that could be obtained during full-scale measurements under the same ambient conditions. Variation of wind orientation produces a wide variance in sample concentrations.

4.4.1 Gas Chromatograph and Integrator

A gas chromatograph (Hewlett-Packard Model 5710A) (GC) with flame ionization detector (FID) operates on the principle that the electrical current produced by the ionization of a gas is directly proportional to the concentration of the molecules being ionized within the gas. The ions in this case are formed by burning the trace gas in a hydrogen-air mixture within the FID. As the electrons are released by the molecules, they move between a set of electrodes, across which a large potential (E) is applied. The resulting electron movement constitutes a small current, which is amplified by an electrometer and passed to a Hewlett-Packard Model 3390A integrator. When no effluent gas is flowing, a carrier gas (nitrogen) flows through the FID. Due to certain impurities in the carrier, some electrons are released, creating a background voltage or zero shift. When the effluent gas enters the FID, the voltage increase

above this zero shift is proportional to the degree of ionization or correspondingly the amount of tracer gas present. Since the chromatograph used in this study features a temperature control on the flame and electrometer, there is very low drift of the zero shift. The HP 3390A integrator, which calculates the area under the effluent peak, also subtracts out the zero drift. The lower limit of measurement is imposed by the instrument sensitivity and the background concentration of trace gases within the air in the wind tunnel. Background concentrations were measured and subtracted from all data given in this report.

4.4.2 Sampling System

The tracer gas sampling system consists of a series of fifty 30 cc syringes mounted between two circular aluminum plates. A variable-speed motor raises a third plate, which lifts the plunger on all 50 syringes, simultaneously. Computer controlled valves and tubing are connected such that airflow from each tunnel sampling point passes by the end of each designated syringe. When the syringe plunger is raised, a sample from the tunnel is drawn into the syringe container. The sampling procedure consists of flushing (taking and expending a sample) the syringe three times after which the test sample is captured. The draw rate is variable and generally set to be approximately 6 cc/min.

The sampling system was periodically calibrated to insure proper function of each of the valves and tubing assemblies. To calibrate the sampler each intake was connected to a manifold. The manifold, in turn, was connected to a gas cylinder having a known concentration of tracer gas. The gas was turned on, and a valve on the manifold was opened to release the pressure produced in the manifold. The manifold was allowed to flush for about one minute. Normal sampling procedures were carried out during calibration to insure exactly the same procedure is reproduced as when taking a sample from the tunnel. Each sample was then analyzed for tracer gas concentration. Percent error was calculated, and "bad" syringe/tube systems (error > 2 percent) were repaired.

4.4.3 Concentration Test Procedure

The concentration test procedure required:

- 1) Setting the proper tunnel wind speed,
- 2) Releasing metered amounts of prepared mixtures of source gases from the various exhaust stacks,
- 3) Withdrawing samples of air from the tunnel designated locations, and
- 4) Analyzing the samples with a FID-GC.

The samples were drawn into each syringe over a 200 second time period and then consecutively injected into the gas chromatograph (GC).

The methodology for analyzing the samples from the tunnel was:

- 1) Introduce the sample into the GC which separates the tracer gases from other hydrocarbons,
- 2) The voltage output from the chromatograph FID electrometer is sent to the HP 3390A Integrator,
- 3) The HP 3390A transmits the measured concentration in ppm to an IBM computer for storage, and
- 4) These values, X_{mea} , along with the response levels for the background X_{bg} and source X_{source} are converted into source normalized model concentration by the equation:

$$X_m = \frac{X_{mea} - X_{bg}}{X_{source} - X_{bg}}$$

- 5) Field equivalent concentration values are related to model values by the equation:

$$X_p = \frac{X_m}{X_m + (1-X_m) \left[\left(\frac{T_a}{T_s} \right)^a V \right]_m / \left[\left(\frac{T_a}{T_s} \right)^a V \right]_p}, \quad \text{where } V = Q/U_H L^2,$$

and L is the characteristic length scale. When there is no distortion in the model-field volume flux ratio, V , and the plumes are isothermal this equation reduces to $X_p = X_m$.

4.4.4 Error Statement

Finite background concentrations, X_{bg} , resulted from previous tests within the laboratory, and these low levels could be measured to accuracies of 20 percent. The larger measured concentrations, X_{mea} , were accurate to 2 percent. The source gas concentration, X_{source} , was known to within 10 percent. Thus the source normalized concentration for $X_{mea} \gg X_{bg}$ was accurate to approximately 10 percent. For low concentration values, $X_{mea} > X_{bg}$, the errors are larger. Values of χ (or K coefficients) listed as being zero in the data tables, (6 through 9) should be interpreted only as being *small*, and not as being absolutely *zero*.

5 VISUALIZATION STUDY RESULTS

A total of 24 test runs were completed on the new School of Pharmacy addition to the University Hospital of Denver Complex. These visualizations are intended to aid in the understanding of the behavior of exhaust plumes. The purpose of these studies is to create a ventilation design which will have a minimal probability of exhaust reentrainment by intake vents within the building complex.

Emissions were simulated from sources on the School of Pharmacy, the School of Medicine (EF-91), the Research Bridge, the Biomedical Research Center, and a single stack on the School of Medicine Annex.

All tests were conducted with the five sources running simultaneously. The test series examined in a progressive order the eight major compass points to evaluate the effect of different wind directions. The wind speed was sequentially increased after every eighth test run while simulated intake and exhaust rates were held constant.

The visualization records were analyzed to note the presence or absence of phenomena, such as;

- * Building downwash - Suction of a plume downward behind a structure or into a building cavity.
- * Plume descent - Deflection of a plume groundward over a building cavity or slightly downwind of a structure.
- * Vortices - Suction of a plume to the side or upwind into a building cavity or in the downwind region of a structure.

Visualization Test Results

1. While the exhaust from the Research Bridge does create a large plume which tends to engulf the entire campus; the clustered buildings between the School of Pharmacy (SOP) and Research Bridge tend to diffuse the exhaust fumes considerably before they reach the SOP site.
2. Exhaust released from buildings on the hospital campus occasionally impinge on the north side of the SOP, but appears to be fairly well diffused, presenting no reason for concern.
3. Exhaust from the SOP with the currently proposed duct configuration is subject to the periodic vortex shedding of the building, which pulls the plume down at regular intervals. This occurrence would subject the intake vents, as modeled, to intermittent reentrainment of exhaust gases. Vortex enhancement occurs for winds coming from the NE, N, and NW.

4. Fumes exiting through the large exhaust stacks on the SOP are subjected to considerable plume decent on the leeward side of the building, however the plume typically does not reattach to the building surface.
5. Fumes exiting through the smaller exhaust stacks on the SOP are also subjected to conditions resulting in plume decent, but since they are located further upwind, the plumes touch down on the SOP roof top and reattach to the building surface. Consequently the flow line followed by material from the small exhaust stacks results in reentrainment by the SOP's intake vents.
6. The exhaust plume from the SOP dips below the roof line of the School of Medicine Annex (SOM Annex), causing its intake vents to be periodically exposed to the SOP's pollutants.

6 CONCENTRATION STUDY RESULTS

Selection of the final intake and exhaust stack configuration for the UCHSC site must be based upon the consideration of its visual appearance, zoning regulations, and minimization of environmental impact. The environmental effects of exhaust from the ventilator stacks will depend upon traffic volume, ventilator flow rates, state and federal ambient air-quality regulations, building and plume aerodynamics, and local meteorology. This study evaluates through fluid modeling the influence of building and plume aerodynamics on plume dilution. Data is reported in terms of normalized concentrations, K , where;

$$K = \chi U_H / Q * 10^7$$

to permit concentration estimates for various exhaust and wind speed conditions. The field and model wind speeds indicated in this table were at equivalent heights of 10 meters. Tables 6 to 9 (and figures 15 to 22) present the normalized concentration data for all tests. This normalized concentration has units of $m^{-2} * 10^7$. This normalized format is convenient because the concentration results, χ , from a test at one particular combination of wind speed, U_H , and flow rate, Q , can be extrapolated to other U_H , Q values provided that the ratio, U_H/Q , remains the same. Note that U_H is the wind speed at 10 meters height approaching the model area and not the value of wind speed above the vent site. The total flow rate, Q , out of the stacks is the exit velocity for a particular run times the total stack exit area.

The results of the concentration tests were examined to note regions of exceptionally high concentrations. The results of this portion of the study are included as part of the following section.

7 DISCUSSION AND RECOMMENDATIONS

The selection of the final intake and exhaust stack configuration must be based upon a balanced consideration of its functional ability, zoning regulations, environmental impact and aesthetic considerations. Based on the combined results of the visualization and concentration studies, several suggestions may be offered.

1. To prevent the touch-down of the SOP's small exhaust effluents the small vents might be incorporated in the larger vents. This could be done by either mixing the effluents before release; or by locating the stacks concentrically, in a telescoping fashion. This would enhance the diffusion of the smaller vents, as well as increasing the effective stack height of the exhaust plumes.
2. The intake vent appears to perform well, in part due to its large intake area. To further decrease the likelihood of exhaust gas reentrainment the intake vent should be made as wide as is reasonably possible, perhaps extending along the full length of the south penthouse wall.
3. The likelihood of exhaust gas reentrainment is greatest for a north to a north-east wind. This is because the effluent is not released at a height sufficient to prevent it from descending, passing in front of the SOP intake, and being re-entrained. Since this study did not distinguish between the large and small diameter exhaust stacks on the SOP, no comment can be made as to their respective contribution of contaminate detected in the SOP intake. To prevent the exhausted material from re-entering the building, the intake vents and exhaust stacks should be centered along the penthouse length. The exhaust stacks (both large and small) being located as nearly as possible to the south edge of the penthouse.
4. Finally, to further decrease the likelihood of exposing the SOM Annex to excessive amounts of the SOP's exhaust, the effective stack height of the SOP exhaust stacks should be increased.

FIGURES

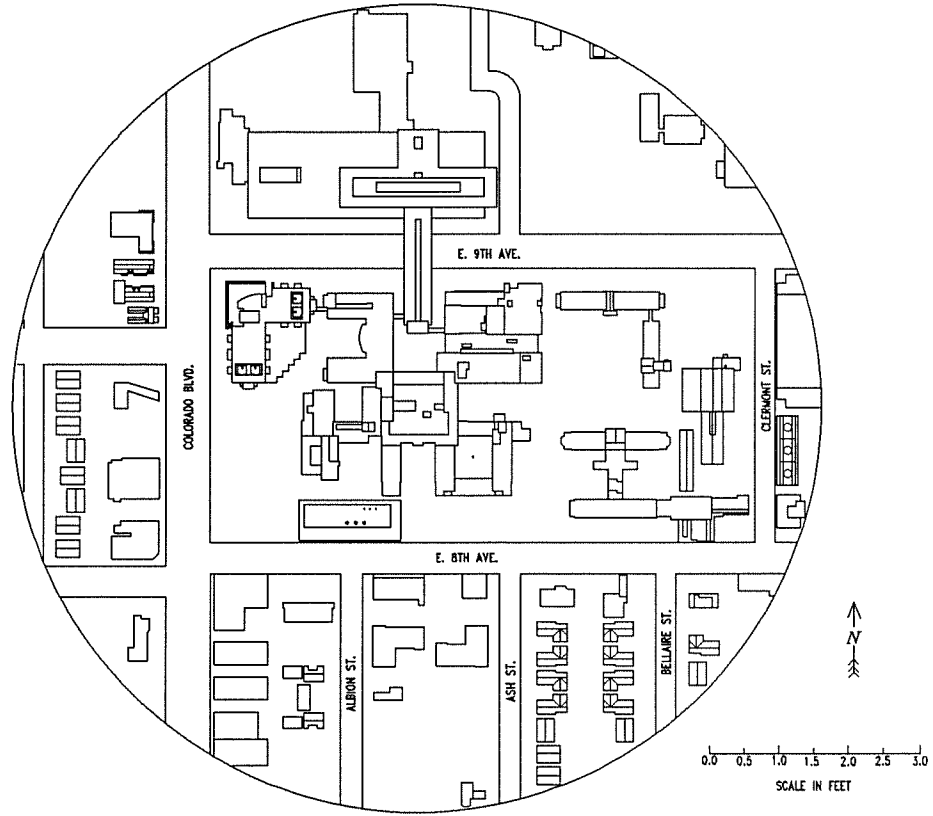


Figure 1 Map of University of Colorado Health Sciences Center

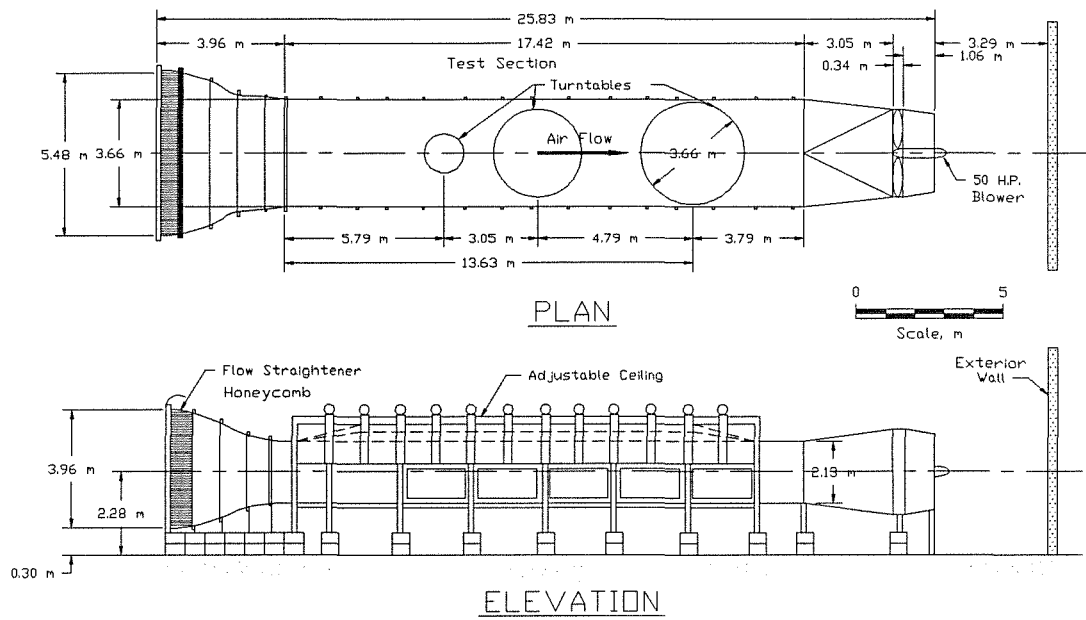


Figure 2 Environmental Wind Tunnel

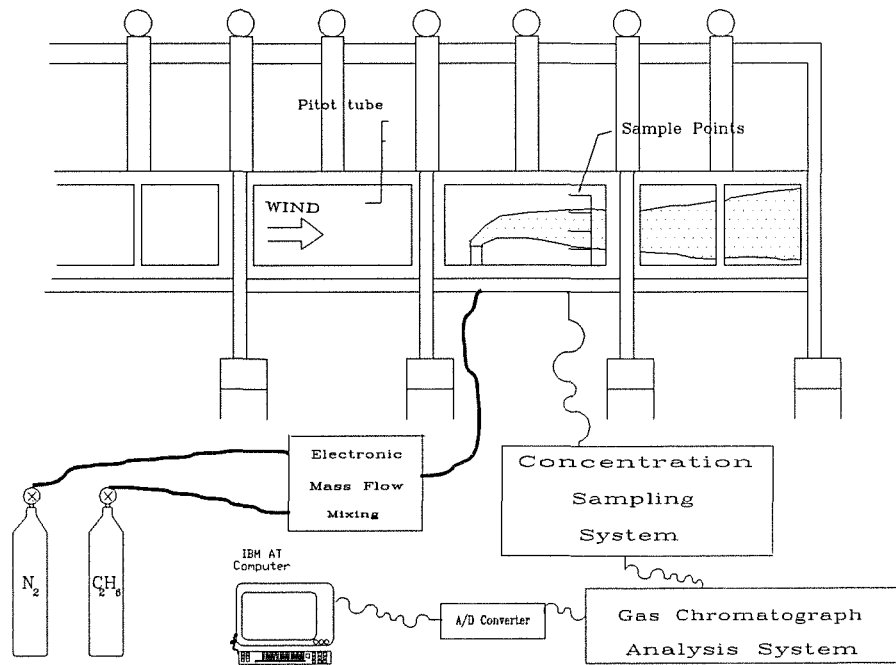


Figure 3 Wind Tunnel Gas Release and Sampling Schematic

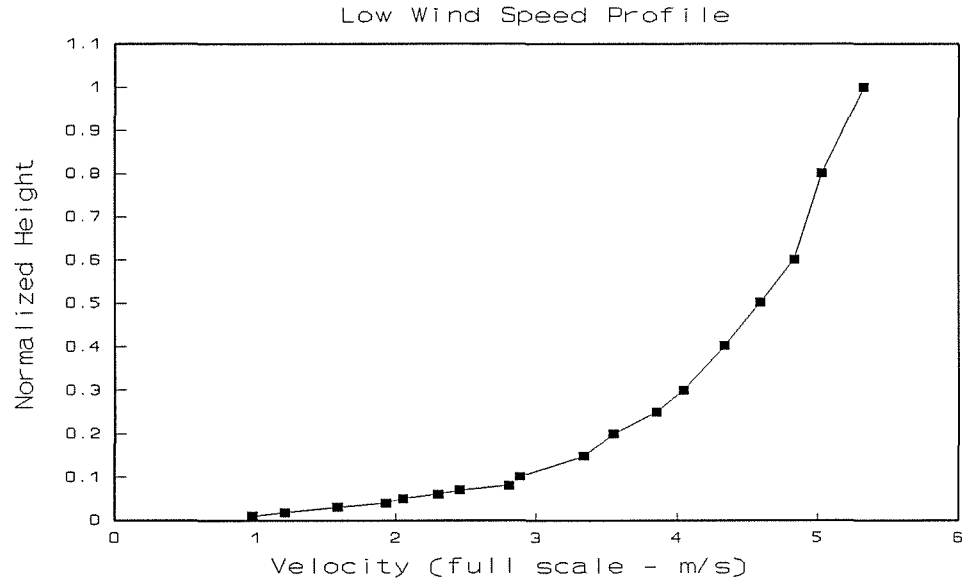


Figure 4

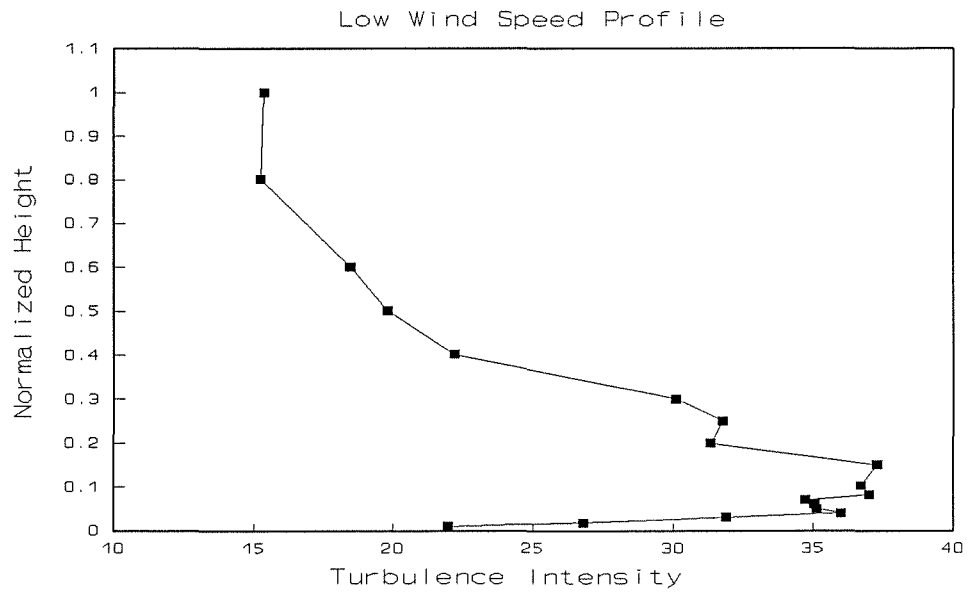


Figure 5

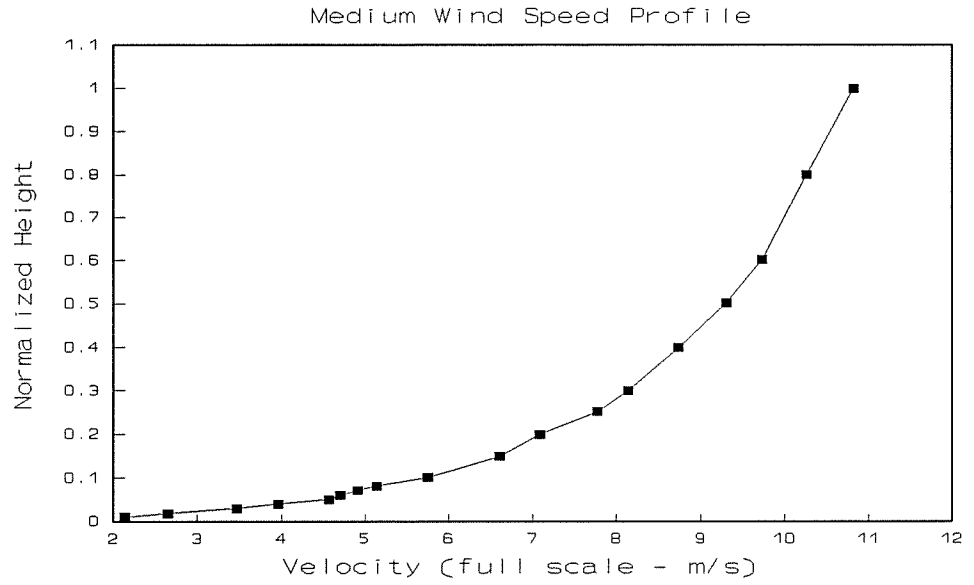


Figure 6

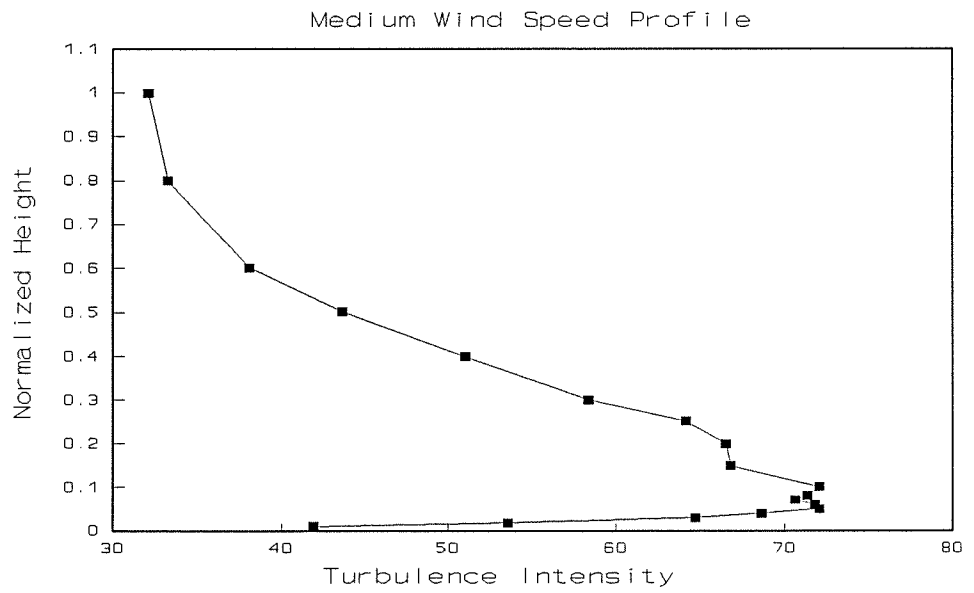


Figure 7

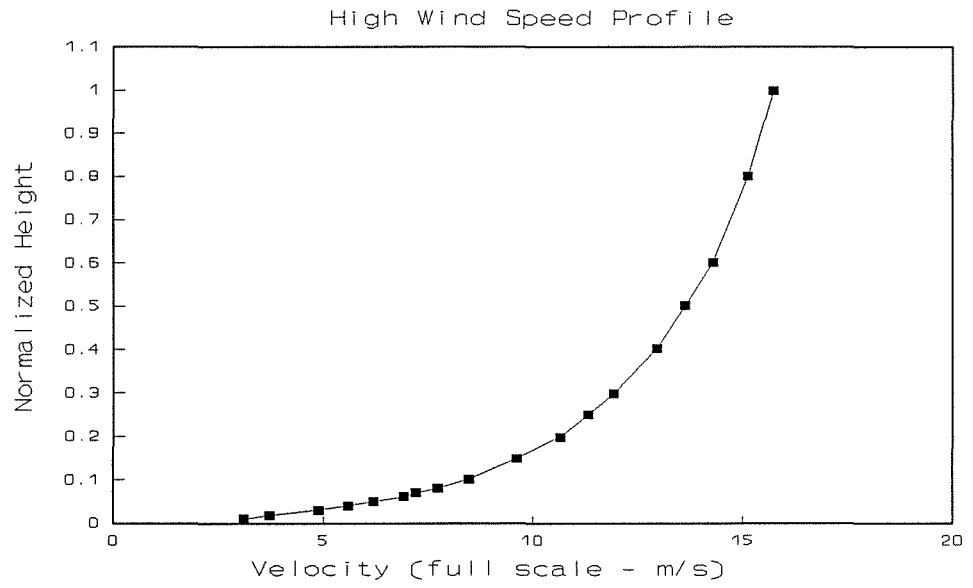


Figure 8

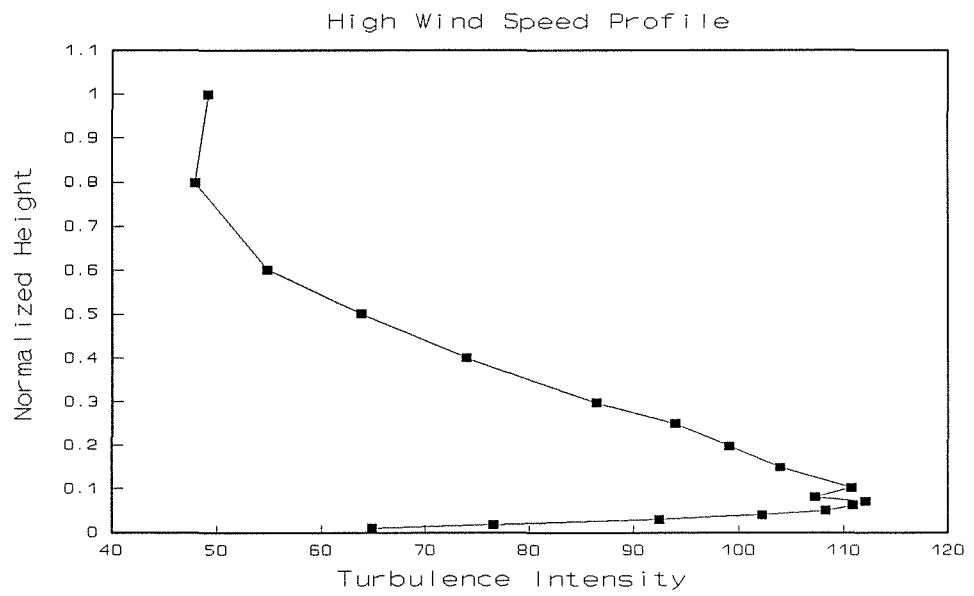


Figure 9

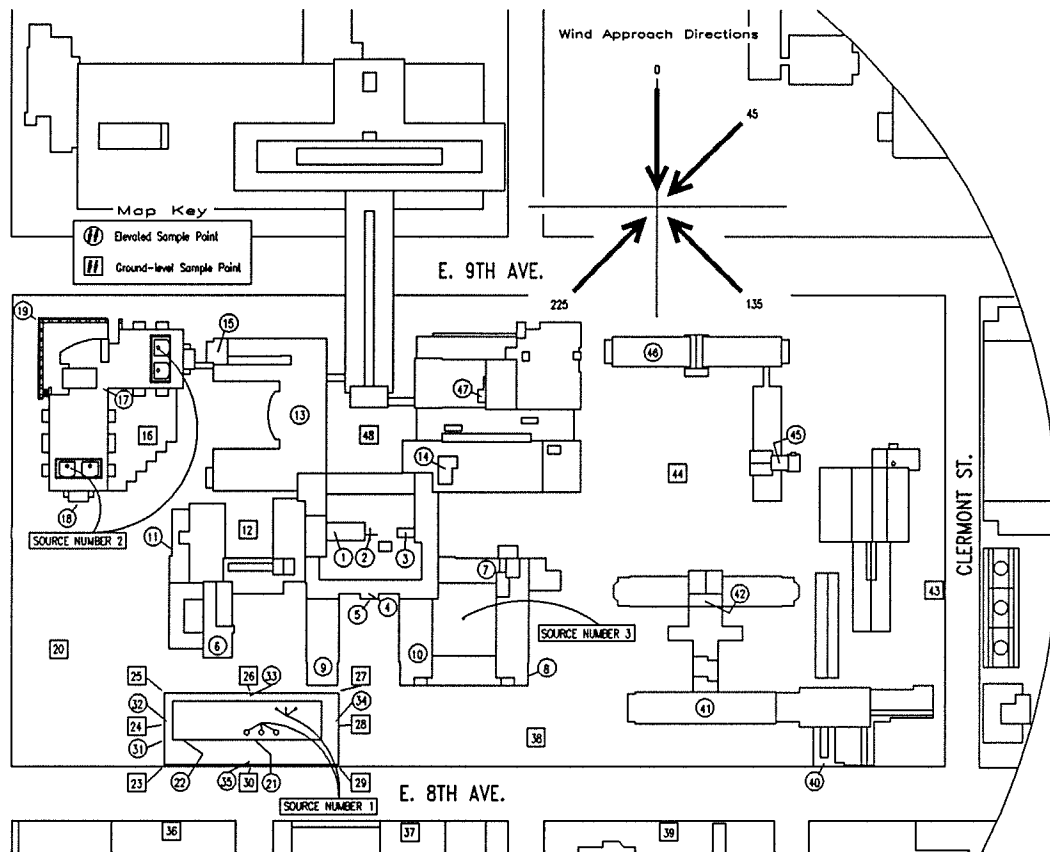


Figure 10 Map of concentration sampling points

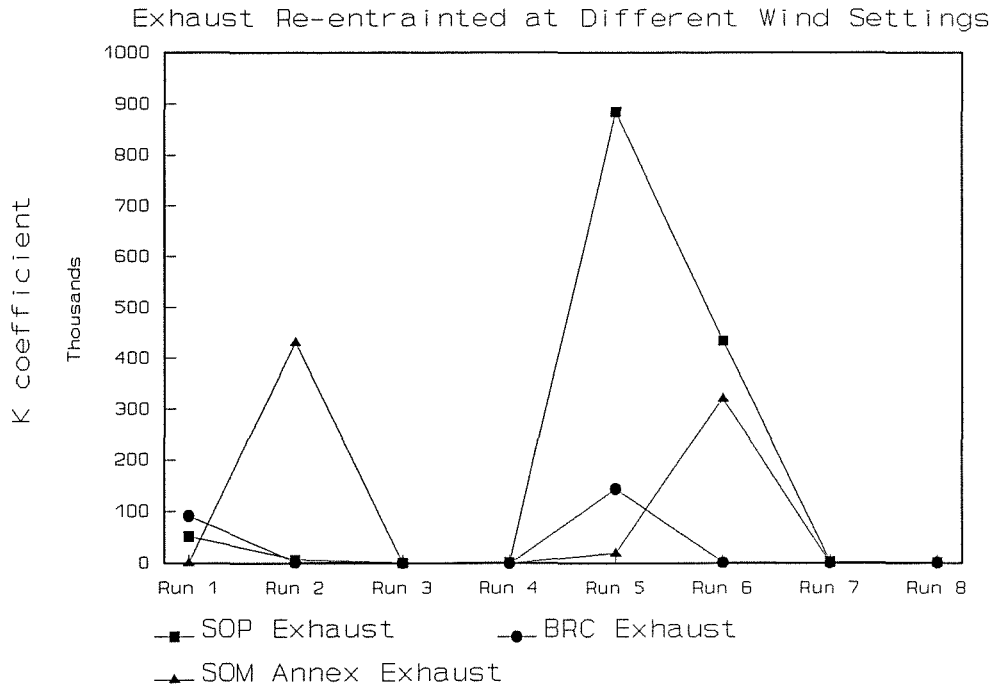


Figure 11 Concentrations Detected at Sampling Point 21

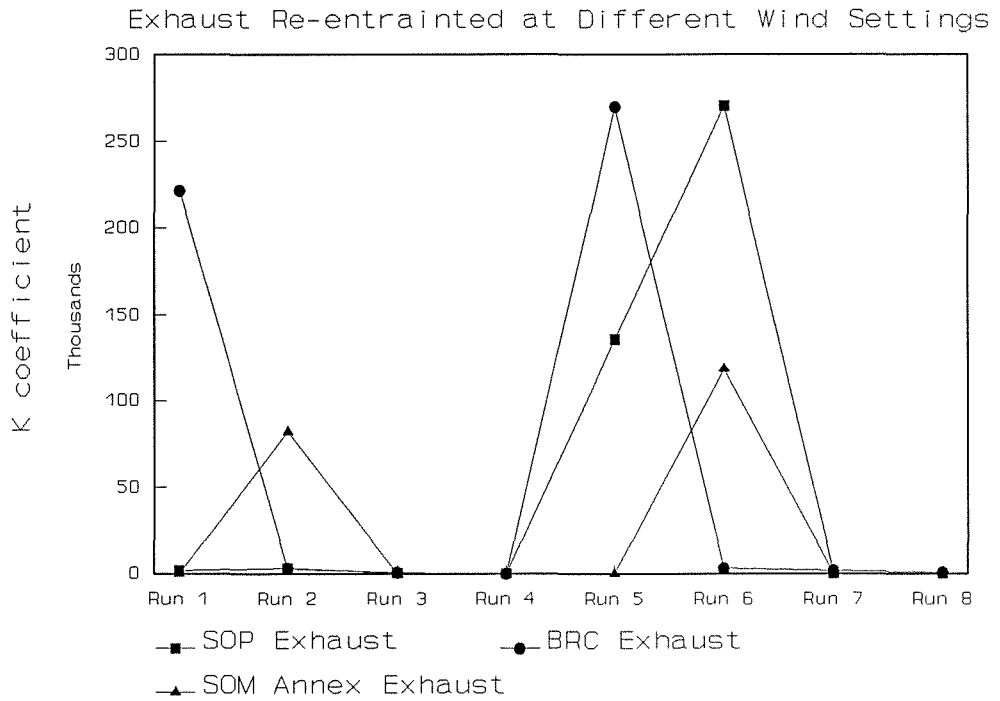


Figure 12 Concentrations Detected at Sampling Point 22

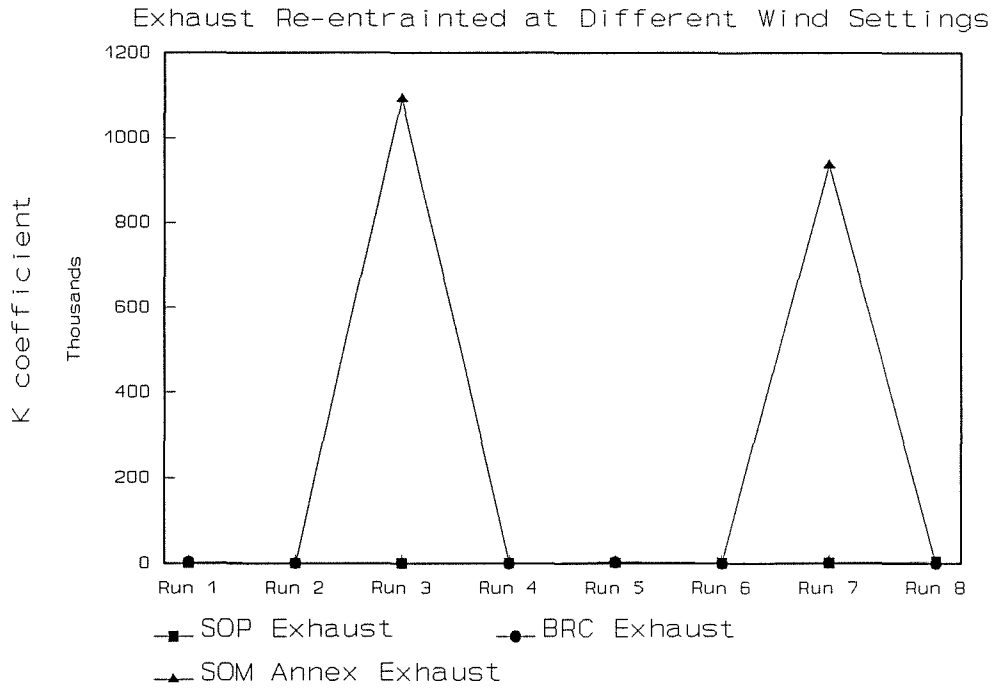


Figure 13 Concentrations Detected at Sampling Point 1

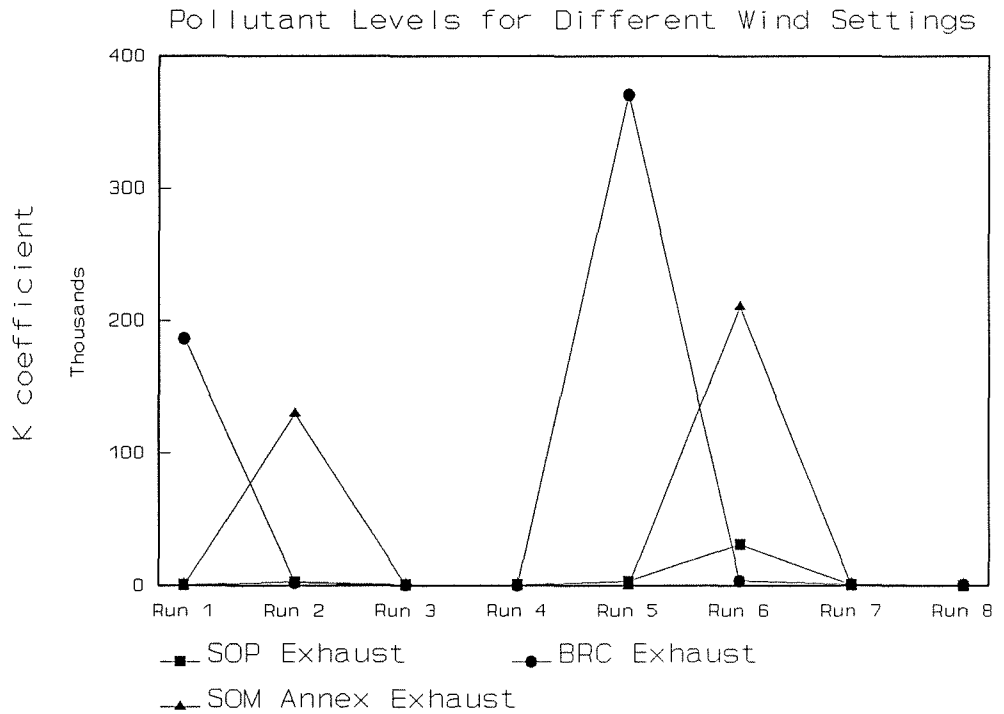


Figure 14 Concentrations Detected at Sampling Point 23

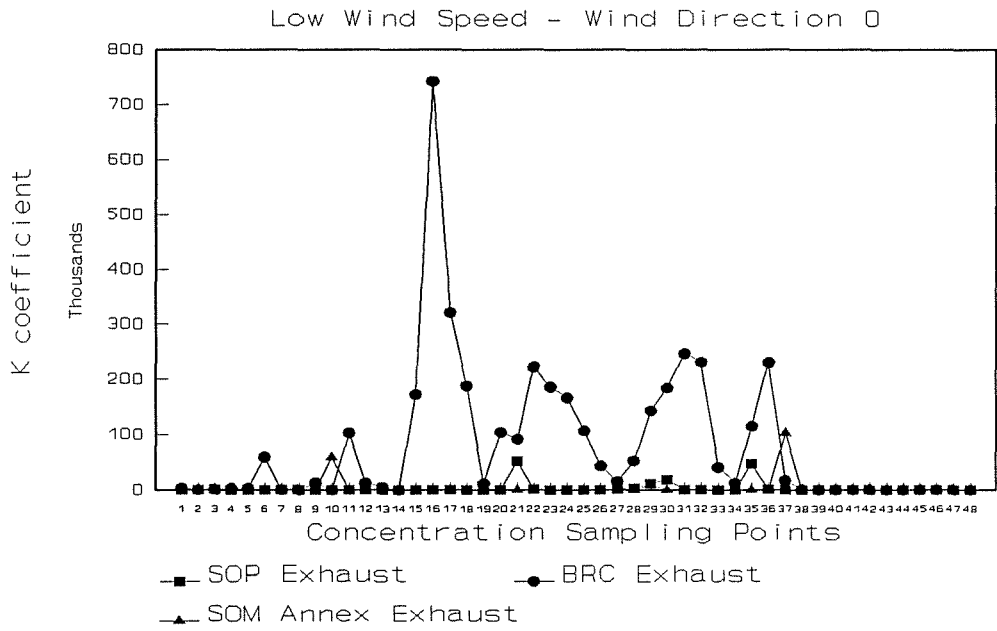


Figure 15

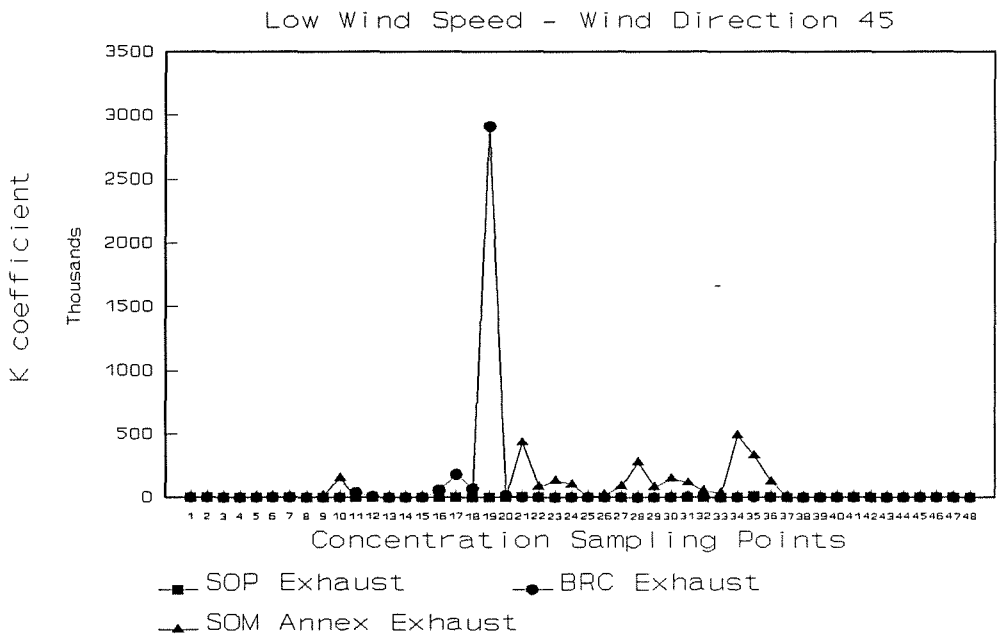


Figure 16

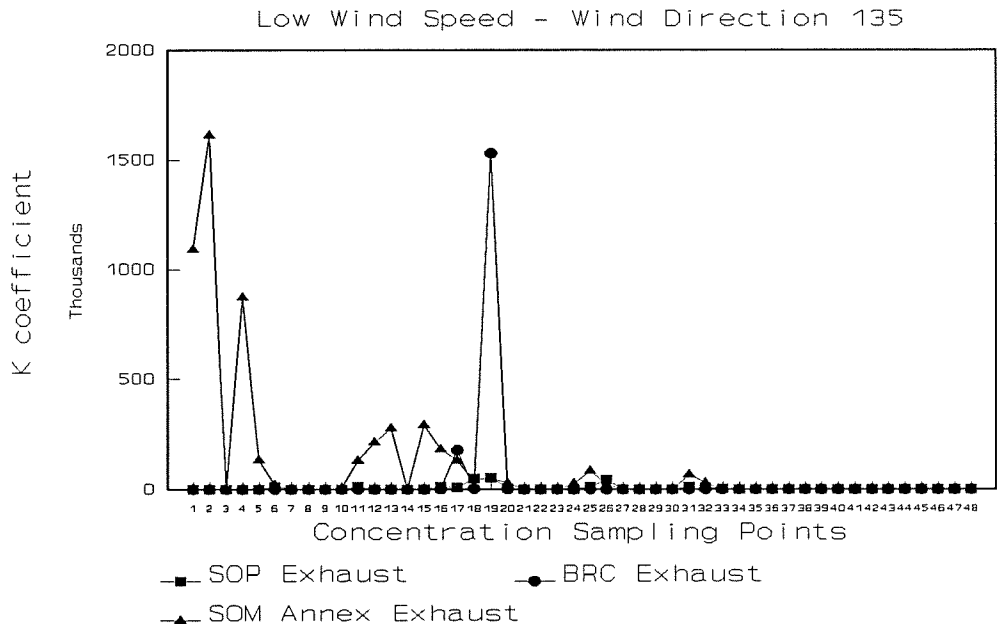


Figure 17

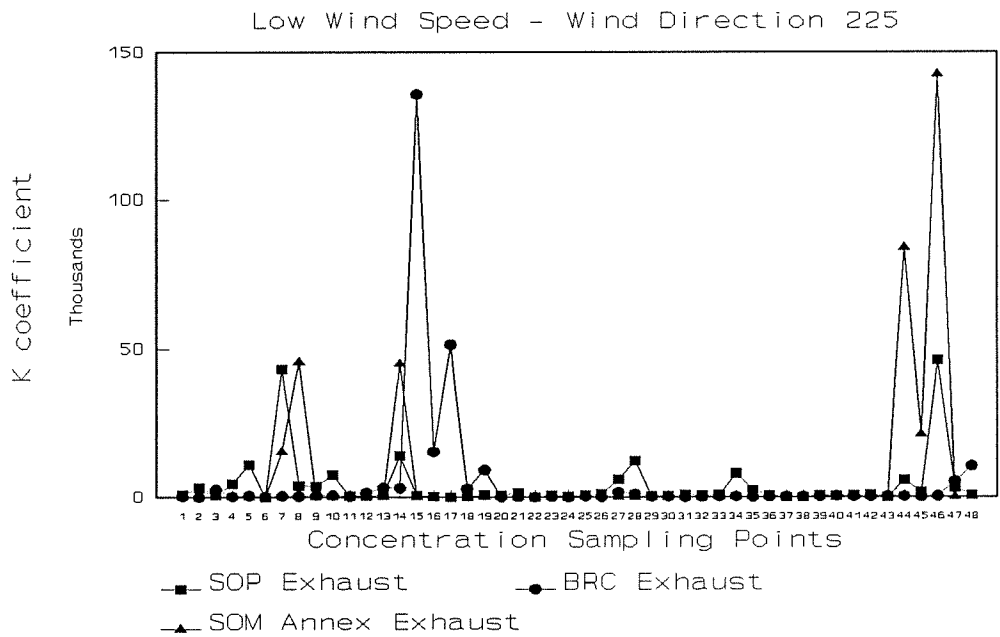


Figure 18

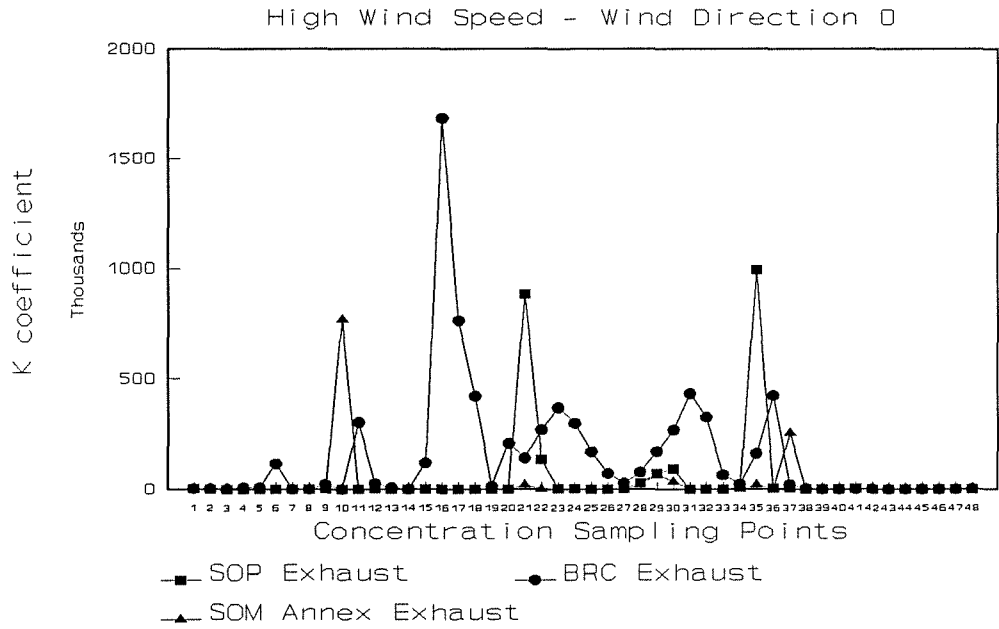


Figure 19

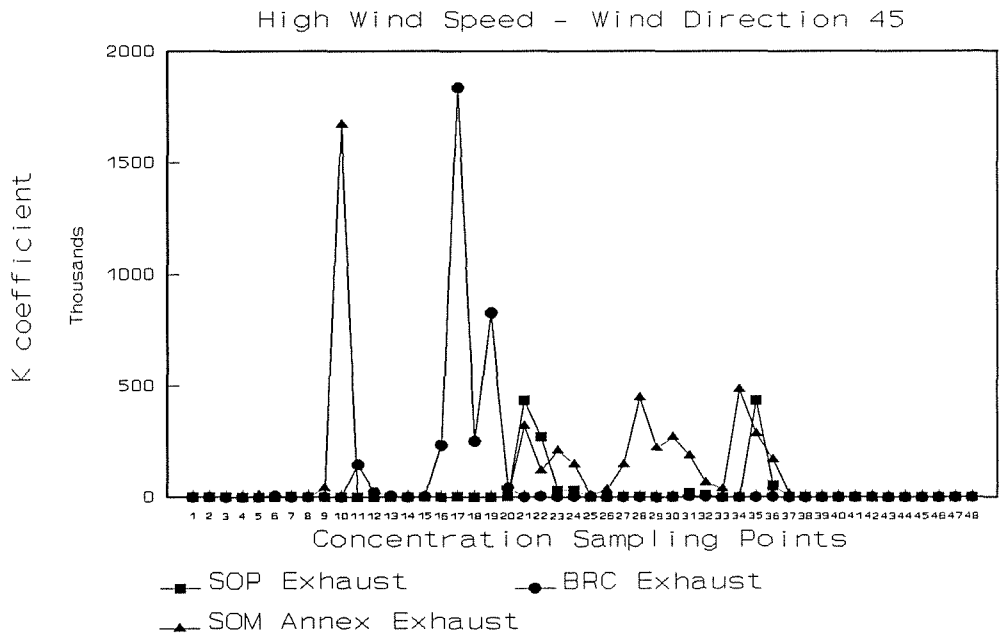


Figure 20

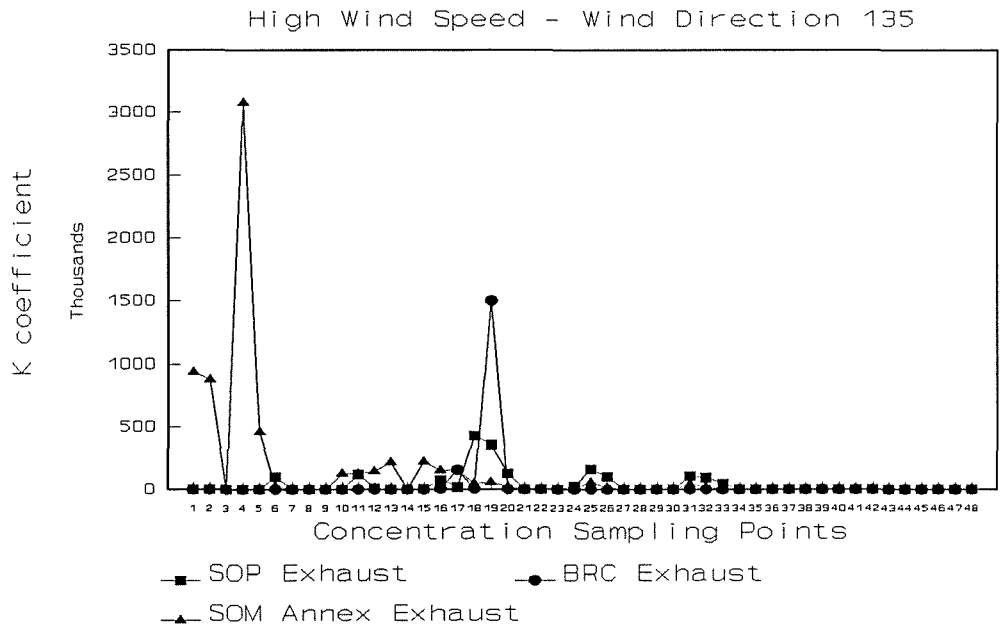


Figure 21

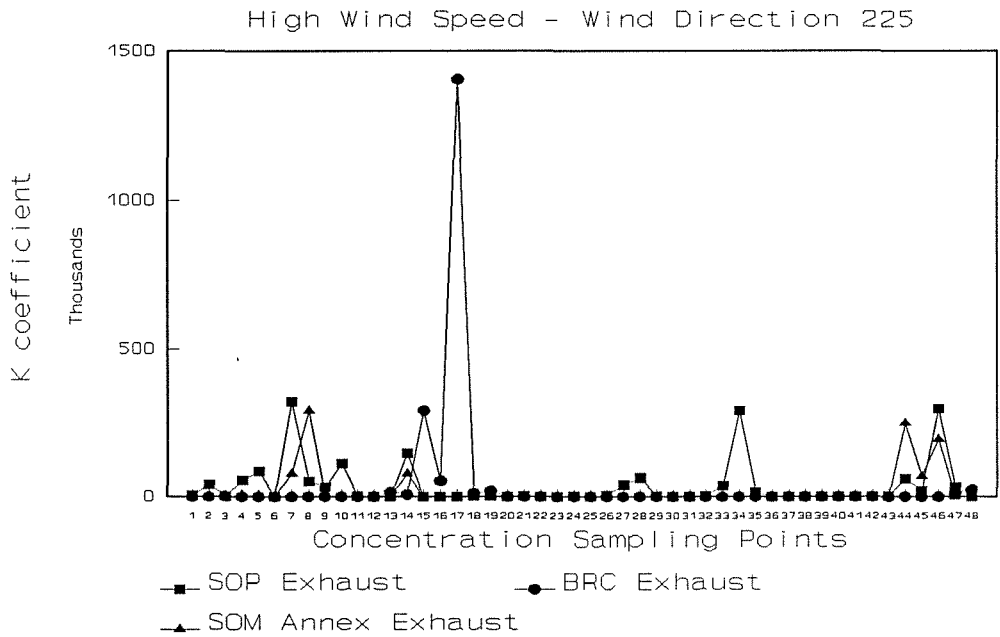


Figure 22

TABLES

Hot-Wire Profile
 Number of points in profile = 18
 Reference Height = 10 m (prototype)
 Reference Velocity = 2.24 m/s (prototype)
 Prototype Height (m) = Normalized Height * 150
 Units of Velocity = m/s (prototype)

Normalized Height	Velocity	Turbulence Intensity
0.01	0.98	21.97
0.02	1.21	26.80
0.03	1.59	31.89
0.04	1.93	35.99
0.05	2.05	35.13
0.06	2.30	35.05
0.07	2.46	34.72
0.08	2.81	37.02
0.10	2.89	36.72
0.15	3.34	37.30
0.20	3.55	31.34
0.25	3.85	31.76
0.30	4.04	30.09
0.40	4.34	22.19
0.50	4.59	19.80
0.60	4.83	18.47
0.80	5.03	15.25
1.00	5.33	15.35

Table 1 Low Wind Speed Profile Data

Hot-Wire Profile
 Number of points in profile = 18
 Reference Height = 10 m (prototype)
 Reference Velocity = 4.51 m/s (prototype)
 Prototype Height (m) = Normalized Height * 150
 Units of Velocity = m/s (prototype)

Normalized Height	Velocity	Turbulence Intensity
0.01	2.14	41.91
0.02	2.65	53.57
0.03	3.47	64.69
0.04	3.96	68.61
0.05	4.57	72.06
0.06	4.70	71.80
0.07	4.91	70.62
0.08	5.14	71.34
0.10	5.76	72.05
0.15	6.61	66.78
0.20	7.09	66.49
0.25	7.77	64.11
0.30	8.14	58.37
0.40	8.73	51.02
0.50	9.31	43.62
0.60	9.73	38.10
0.80	10.26	33.26
1.00	10.82	32.09

Table 2 Medium Wind Speed Profile Data

Hot-Wire Profile
 Number of points in profile = 18
 Reference Height = 10 m (prototype)
 Reference Velocity = 6.61 m/s (prototype)
 Prototype Height (ft) = Normalized Height * 492
 Units of Velocity = m/s (prototype)

Normalized Height	Velocity	Turbulence Intensity
0.01	3.09	64.85
0.02	3.71	76.56
0.03	4.88	92.46
0.04	5.59	102.19
0.05	6.20	108.26
0.06	6.92	110.86
0.07	7.21	112.08
0.08	7.74	107.27
0.10	8.49	110.74
0.15	9.63	103.93
0.20	10.65	99.08
0.25	11.32	93.94
0.30	11.93	86.38
0.40	12.96	73.90
0.50	13.64	63.80
0.60	14.30	54.79
0.80	15.13	47.93
1.00	15.72	49.16

Table 3 High Wind Speed Profile Data

VISUALIZATION TEST PLAN

Wind Speed is given in full scale (prototype) units of miles per hour.
Wind Direction is given as the compass direction the wind flows *from*.

<u>Run Number</u>	<u>Wind Speed</u>	<u>Wind Direction</u>
1	5	North (N)
2	5	North-East (NE)
3	5	East (E)
4	5	South-East (SE)
5	5	South (S)
6	5	South-West (SW)
7	5	West (W)
8	5	North-West (NW)
9	10	N
10	10	NE
11	10	E
12	10	SE
13	10	S
14	10	SW
15	10	W
16	10	NW
17	15	N
18	15	NE
19	15	E
20	15	SE
21	15	S
22	15	SW
23	15	W
24	15	NW

Flows simulated

Total School of Pharmacy exhaust rate: 250 000 cfm
School of Pharmacy intake rate: 250 000 cfm
Total Biomedical Research Center exhaust rate: 40 000 cfm
Research Bridge exhaust rate: 161 600 cfm
School of Medicine exhaust rate: 6200 cfm
School of Medicine, Large vent well intake rate: 272 700 cfm
School of Medicine, Small vent well intake rate: 120 300 cfm
School of Medicine Annex exhaust rate: 4800 cfm
School of Medicine Annex intake rate: 119 200

Table 4

CONCENTRATION TEST PLAN

Wind Speed is given in full scale (prototype) units of miles per hour.
Wind Direction is given as the compass direction the wind flows *from*.

<u>Run Number</u>	<u>Wind Speed</u>	<u>Wind Direction</u>
1	5	North (N)
2	5	North-East (NE)
3	5	South-East (SE)
4	5	South-West (SW)
5	15	N
6	15	NE
7	15	SE
8	15	SW

Flows simulated

Total School of Pharmacy exhaust rate: 250 000 cfm

School of Pharmacy intake rate: 250 000 cfm

Total Biomedical Research Center exhaust rate: 40 000 cfm

School of Medicine, Large vent well intake rate: 272 700 cfm

School of Medicine, Small vent well intake rate: 120 300 cfm

School of Medicine Annex exhaust rate: 4800 cfm

School of Medicine Annex intake rate: 119 200

Table 5

For the following tables, the column headings are:

Kp 1 K coefficient for the SOP exhaust

Kp 2 K coefficient for the BRC exhaust

Kp 3 K coefficient for the SOM Annex exhaust

Point No.	X(ft)	Y(ft)	Z(ft)	Run 1			Run 2		
				Kp 1	Kp 2	Kp 3	Kp 1	Kp 2	Kp 3
1	-50	8	59	29	2746	0	307	430	0
2	0	0	79	0	179	0	534	186	0
3	45	4	58	713	781	0	742	0	0
4	0	-69	58	0	3506	0	519	616	0
5	0	-75	5	0	3506	0	0	129	5436
6	-151	-138	46	289	59448	0	446	1577	3395
7	151	-44	58	152	50	0	762	43	0
8	136	-101	45	0	0	0	0	215	0
9	-60	-171	58	0	12928	0	224	388	12335
10	79	-160	63	243	653	58748	677	0	151155
11	-248	-10	5	65	103228	0	111	36568	0
12	-155	3	0	639	12139	0	39	7256	0
13	-95	144	58	21	5141	0	0	860	0
14	98	81	46	0	251	0	0	0	0
15	-189	215	70	0	172292	0	0	1649	0
16	-293	115	-1	0	741787	0	317	57978	0
17	-333	168	74	0	320871	0	309	180229	0
18	-367	40	6	0	188252	0	332	69594	0
19	-414	248	10	146	11723	0	0	2912489	0
20	-392	-145	0	0	103816	0	0	18255	0
21	-143	-275	83	51639	91814	0	6496	1420	431494
22	-230	-275	83	1685	221593	0	2964	2925	82014
23	-252	-306	0	612	186445	0	2976	2466	129721
24	-252	262	0	10	166355	0	1813	2194	99137
25	-252	-218	0	4	106828	0	93	1620	5874
26	-143	-218	0	0	43659	0	461	287	20727
27	-33	-218	0	716	14993	0	344	186	84383
28	-33	-262	0	3640	53453	0	983	689	275112
29	-33	-306	0	11766	143181	9318	338	1850	79854
30	-143	-306	0	18429	184165	0	752	2050	144156
31	-252	-283	39	189	246015	0	584	3700	113135
32	-251	-262	78	17	230240	0	646	3915	51211
33	-143	-219	78	293	41121	0	540	444	33013
34	-34	-262	78	62	12498	0	0	258	491257
35	-143	-305	78	47900	115016	0	10118	1262	325835
36	-250	-372	0	867	229953	0	536	2897	118949
37	50	-376	0	393	17316	102154	0	0	0
38	209	-256	0	0	1227	0	523	0	0
39	378	-375	0	520	207	0	382	0	0
40	590	-298	15	335	337	0	0	0	0
41	438	-229	31	0	322	0	590	0	0
42	441	-229	31	449	165	0	665	0	0
43	710	-73	0	0	623	0	0	0	0
44	410	81	0	0	395	0	182	0	0
45	525	84	38	212	0	0	251	0	0
46	381	225	33	0	294	0	186	0	0
47	151	143	44	304	351	0	88	14	0
48	-3	126	0	135	50	0	536	129	0

Table 6

Point No.	X(ft)	Y(ft)	Z(ft)	Run 3			Run 4		
				Kp 1	Kp 2	Kp 3	Kp 1	Kp 2	Kp 3
1	-50	8	59	347	531	1091278	851	244	0
2	0	0	79	27	344	1611446	3129	14	0
3	45	4	58	524	602	1722	601	2524	0
4	0	-69	58	674	459	872117	4445	258	0
5	0	-75	5	412	517	132678	11019	517	0
6	-151	-138	46	9445	602	21972	77	158	0
7	151	-44	58	666	459	0	43166	473	15292
8	136	-101	45	175	501	0	3850	402	45557
9	-60	-171	58	397	459	0	3578	689	0
10	79	-160	63	19	416	4629	7641	645	0
11	-248	-10	5	10751	1448	130308	337	388	0
12	-155	3	0	1772	788	211944	464	1521	0
13	-95	144	58	576	473	275699	578	3256	0
14	98	81	46	412	388	0	14043	3112	45019
15	-189	215	70	984	645	291319	647	135801	0
16	-293	115	-1	10391	2782	180066	135	15373	0
17	-333	168	74	7496	178235	129014	89	51481	0
18	-367	40	6	49600	4201	39095	220	2825	0
19	-414	248	10	50278	1531509	49967	817	9321	0
20	-392	-145	0	5509	1792	27567	626	101	0
21	-143	-275	83	630	745	0	1419	143	0
22	-230	-275	83	306	745	0	0	0	0
23	-252	-306	0	653	660	0	699	230	0
24	-252	262	0	1519	745	24988	200	0	0
25	-252	-218	0	12482	1105	84005	589	244	0
26	-143	-218	0	43261	487	19174	1023	43	0
27	-33	-218	0	320	416	0	6047	1749	0
28	-33	-262	0	39	373	0	12238	1133	0
29	-33	-306	0	728	531	0	466	273	0
30	-143	-306	0	493	631	0	358	258	0
31	-252	-283	39	9938	1248	66443	803	87	0
32	-251	-262	78	7604	990	28433	674	158	0
33	-143	-219	78	2471	258	0	969	287	0
34	-34	-262	78	337	200	0	8096	301	0
35	-143	-305	78	1123	574	0	2382	43	0
36	-250	-372	0	214	788	0	587	172	0
37	50	-376	0	749	344	0	4	244	0
38	209	-256	0	114	200	0	94	287	0
39	378	-375	0	341	301	0	670	402	0
40	590	-298	15	193	416	0	362	459	0
41	438	-229	31	196	315	0	570	273	0
42	441	-229	31	206	301	0	791	315	0
43	710	-73	0	454	358	0	0	444	0
44	410	81	0	545	215	0	5910	315	84005
45	525	84	38	152	358	0	1598	200	21215
46	381	225	33	389	287	0	46130	344	142583
47	151	143	44	354	301	0	3120	5363	0
48	-3	126	0	0	315	0	676	10568	0

Table 7

Point No.	X(ft)	Y(ft)	Z(ft)	Run 5			Run 6		
				Kp 1	Kp 2	Kp 3	Kp 1	Kp 2	Kp 3
1	-50	8	59	2147	3797	0	1161	599	0
2	0	0	79	0	2038	0	595	471	0
3	45	4	58	454	2765	0	2542	557	0
4	0	-69	58	255	7483	0	812	1028	0
5	0	-75	5	566	9199	0	320	386	9499
6	-151	-138	46	1033	117030	0	1136	5360	804
7	151	-44	58	1077	1223	0	2219	0	0
8	136	-101	45	1220	1567	0	513	0	0
9	-60	-171	58	1923	22755	0	986	599	39128
10	79	-160	63	890	964	767284	1441	429	1669670
11	-248	-10	5	1095	304042	953	1671	147680	0
12	-155	3	0	2047	27002	0	1266	21833	0
13	-95	144	58	19	7398	0	588	5920	0
14	98	81	46	1599	1095	2888	856	344	0
15	-189	215	70	970	120164	0	0	2357	0
16	-293	115	-1	1599	1683246	0	538	234021	0
17	-333	168	74	0	764232	0	1789	1836534	0
18	-367	40	6	0	422040	0	0	252636	0
19	-414	248	10	834	13747	0	1503	828212	0
20	-392	-145	0	0	209894	0	3196	42806	804
21	-143	-275	83	884197	143883	19326	434938	1414	320022
22	-230	-275	83	135309	269730	0	270124	3088	118367
23	-252	-306	0	3311	370783	0	31352	3818	210499
24	-252	262	0	2937	300266	0	31950	4289	146715
25	-252	-218	0	56	171204	0	656	2918	8844
26	-143	-218	0	1095	72165	0	1634	599	34632
27	-33	-218	0	3204	27945	0	1870	900	145435
28	-33	-262	0	29576	77915	20279	4061	642	446935
29	-33	-306	0	71186	172105	65392	1055	1244	220802
30	-143	-306	0	92355	269858	34453	2710	2574	271067
31	-252	-283	39	1468	434390	0	18849	5661	188285
32	-251	-262	78	1637	327935	0	12444	4591	66196
33	-143	-219	78	0	65433	0	1080	471	37848
34	-34	-262	78	7324	23783	0	1173	0	483025
35	-143	-305	78	993590	163271	19326	434745	1716	284259
36	-250	-372	0	5874	426843	0	53485	4417	168959
37	50	-376	0	6434	21553	256089	2710	0	14323
38	209	-256	0	124	2467	655	1957	0	0
39	378	-375	0	1475	1007	0	433	0	0
40	590	-298	15	0	450	0	899	0	0
41	438	-229	31	1805	922	0	0	0	0
42	441	-229	31	0	238	0	240	0	0
43	710	-73	0	1637	106	0	1354	0	0
44	410	81	0	181	922	0	545	0	0
45	525	84	38	616	493	0	271	0	0
46	381	225	33	1773	752	2888	576	170	0
47	151	143	44	1637	1007	0	90	0	0
48	-3	126	0	865	2123	0	439	1071	0

Table 8

Point No.	X(ft)	Y(ft)	Z(ft)	Run 7			Run 8		
				Kp 1	Kp 2	Kp 3	Kp 1	Kp 2	Kp 3
1	-50	8	59	1211	1737	936064	3948	0	0
2	0	0	79	0	1567	875169	40619	386	0
3	45	4	58	1528	2680	0	1864	2017	0
4	0	-69	58	0	1049	3077801	55858	471	5152
5	0	-75	5	115	620	457416	85180	730	3544
6	-151	-138	46	102727	1737	26413	1061	471	0
7	151	-44	58	899	964	0	322881	0	77631
8	136	-101	45	0	620	0	51104	943	291197
9	-60	-171	58	364	149	0	33631	1028	0
10	79	-160	63	0	1049	125305	111097	943	0
11	-248	-10	5	118664	3024	124322	2200	858	0
12	-155	3	0	11690	1567	147192	0	1287	0
13	-95	144	58	974	1138	215829	744	14928	0
14	98	81	46	0	365	2591	146703	7164	77958
15	-189	215	70	6338	2166	222916	1248	292354	328
16	-293	115	-1	73472	6884	149782	488	54430	0
17	-333	168	74	16911	156493	157524	265	1405887	0
18	-367	40	6	426487	5427	46721	1895	10936	0
19	-414	248	10	355986	1502594	52498	1783	19129	0
20	-392	-145	0	123344	2467	19326	513	429	0
21	-143	-275	83	2162	879	0	1546	900	0
22	-230	-275	83	90	1524	0	0	773	0
23	-252	-306	0	619	1223	0	0	642	0
24	-252	262	0	24677	1266	9350	1422	815	0
25	-252	-218	0	161945	1351	53153	165	429	0
26	-143	-218	0	100126	752	15782	4322	386	0
27	-33	-218	0	943	280	0	40183	943	0
28	-33	-262	0	0	493	0	63917	1028	0
29	-33	-306	0	0	191	0	1907	599	0
30	-143	-306	0	0	1308	0	756	900	0
31	-252	-283	39	106878	1953	39307	968	900	0
32	-251	-262	78	92746	2209	21261	1807	815	0
33	-143	-219	78	44106	879	1936	37084	0	0
34	-34	-262	78	47	0	655	291095	773	0
35	-143	-305	78	1665	837	0	14820	642	0
36	-250	-372	0	0	2294	0	445	1159	0
37	50	-376	0	0	238	0	1005	0	0
38	209	-256	0	109	493	0	1266	0	0
39	378	-375	0	109	493	0	0	557	0
40	590	-298	15	0	794	0	0	730	0
41	438	-229	31	128	1138	0	0	642	0
42	441	-229	31	0	620	0	246	642	0
43	710	-73	0	40	1049	0	1384	773	0
44	410	81	0	0	964	0	60911	514	249002
45	525	84	38	0	535	0	20345	85	69591
46	381	225	33	376	1308	0	297953	128	193913
47	151	143	44	271	1180	0	31814	12482	328
48	-3	126	0	0	1822	1936	0	23634	0

Table 9

REFERENCES

- Allwine, K. J., Meroney, R. N., Peterka, J. A. (1978), "Rancho Seco Building Wake Effects on Atmospheric Diffusion: Simulation in a Meteorological Wind Tunnel," FDDL Report CER77-78KJA-RNM-JAP25, CSU, Fort Collins, Colorado.
- Arya, S. P. S., and Plate, E. J. (1969), "Modeling of the Stably Stratified Atmospheric Boundary Layer," *J. Atmos. Sci.*, Vol. 26, No. 4, pp. 656-665.
- Arya, S. P. S. (1975), "Buoyancy Effects in a Horizontal Flat-Plate Boundary Layer," *J. Fluid Mech.*, Vol. 68, Pt. 2, pp. 321-343.
- Barad, M. L., ed. (1958), "Project Prairie Grass: A Field Program in Diffusion," Geophysical Research Papers, No. 59, Vols. I and II, Report AFCRC-TR-58-235, Air Force Cambridge Research Center.
- Cermak, J. E. (1975), "Applications of Fluid Mechanics to Wind Engineering--A Freeman Scholar Lecture," *J. of Fluids Engineering*, Vol. 97, pp. 9-38.
- Cermak, J. E. (1990), "Atmospheric Boundary Layer Modelling in Wind Tunnels," Proceedings of the Symposium on Experimental Determination of Wind Loads on Civil Engineering Structures, Delhi, India, December 1990.
- Cermak, J. E., Peterka, J. A. (1985), "Wind-Tunnel Study of Exhaust-Intake Cross Contamination and Dispersion of Rooftop Emissions, Hospital of the University of Pennsylvania," FDDL Report CER84-85JEC-JAP1, CSU, Fort Collins, Colorado.
- Cermak, J. E., Shrivastava, P. K., Poreh, M. (1983), "Wind-tunnel Research on the Mechanics of Plumes in the Atmospheric Surface Layer," FDDL Report CER83-84JEC-PKS-MP12, CSU, Fort Collins, Colorado, Annual Progress Report to U.S. Dept. of Army Contract DAAK11-82-K-0004, 140 pp.
- Chaudhry, F. H. Meroney, R. N. (1973), "A Laboratory Study of Diffusion in Stably Stratified Flow," Atmospheric Environment, Vol. 7, pp. 443-454.
- Counihan, J. (1975), "Adiabatic Atmospheric Boundary Layers: A Review and Analysis of Data from the Period 1880-1972," *Atmos. Envir.*, Vol. 9, pp. 871-905.
- Fage, A., Warsap, J. H. (1929), "Effects of Turbulence and Surface Roughness on Drag of Circular Cylinders," U.K., ARC R&M 1283.
- Farell, C., Carrasquel, S., Guven, O., Patel, V. C. (1977), "Effect of Wind-Tunnel Walls on the Flow Past Circular Cylinders and Cooling Tower Models," *J. of Fluids Engineering*, Vol. 99, pp. 470-479.
- Gifford, F. A. (1976), "Turbulent Diffusion-Typing Schemes: A Review," *Nucl. Saf.*, Vol. 17, No. 1, pp. 72 ff.
- Golden, J. (1961), "Scale Model Techniques," M.S. Thesis, Dept. of Meteorology and Oceanography, New York University, 42 pp.
- Golder, D. G. (1972), "Relations Among Stability Parameters in the Surface Layer," *Boundary-Layer Meteorology*, Vol. 3, No. 1, pp. 47-58.
- Halitsky, J. (1968), "Gas Diffusion Near Buildings," *Meteorology and Atomic Energy*, 1968, editor D. H. Slade, Atomic Energy Commission, Ch. 5-5, pp. 221-256.
- Hatcher, R. V., Meroney, R. N. (1977), "Dispersion in the Wake of a Model Industrial Complex," Joint Conference on Applications of Air Pollution Meteorology, Proceedings, Am. Meteorol. Soc., Salt Lake City, Utah, 29 November - 2 December, 1977, pp. 343-346.
- Haugen, D. A., Kaimal, J. C., Bradley, E. F. (1971), "An Experimental Study of Reynolds Stress and Heat Flux in the Atmospheric Surface Layer," *Quart. J. Roy. Meteorol. Soc.*, Vol. 97, pp. 168-180.
- Hinze, J. O. (1975), Turbulence, McGraw-Hill, New York, 2nd. edition, 790 pp.

- Horst, T. W. (1979), "Lagrangian Similarity Modeling of Vertical Diffusion from a Ground Level Source," J. Appl. Meteorol., Vol. 18, pp. 733-740.
- Hosker, R. P., Jr. (1984), "Flow and Diffusion Near Obstacles," Atmospheric Science and Power Production, DOE/TIC-27601, pp. 241-326.
- Hsi, G., Cermak, J. E. (1965), "Meteorological-Tower Induced Wind Field Perturbations," Prepared under U.S. Army Research Grant DA-AMC-28-043-64-G-9, FDDL Report CER65-GH-JEC49, CSU, Fort Collins, Colorado.
- Huber, A. H. (1989), "The Influence of Building Width and Orientation on Plume Dispersion in the Wake of a Building," Atmospheric Research and Exposure Assessment Laboratory, U.S. EPA, Research Triangle Park, NC 27711, pp. 2109-2116.
- Hunt, J. C. R. (1974), "Wakes Behind Buildings," presented at the Aeronautical Research Council's Atmospheric Environment Committee Meeting, Oct. 23, ARC Report 35601, Atmos. 229, Aeronautical Research Council of Great Britain, Her Majesty's Stationery Office, London.
- Hunt, J. C. R., Snyder, W. H., and Lawson, F. E., Jr. (1978), "Flow Structure and Turbulent Diffusion around a Three-Dimensional Hill: Fluid Modeling Study on Effects of Stratification: Part I: Flow Structure," Envir. Prot. Agcy. Report No. EPA 600/4-78-041, Research Triangle Park, NC, 84 pp.
- Islitzer, N. F. and Dumbauld, R. K. (1963), "Atmospheric Diffusion Deposition Studies over Flat Terrain," Int. J. Air Water Pollut., Vol. 7 (11-12), pp. 999-1022.
- Kline, S. J. (1965), Similitude and Approximation Theory, McGraw-Hill Book Company, New York, 229 pp.
- Kothari, K. M., Meroney, R. N., Bouwmeester, (1981), "An Algorithm to Estimate Field Concentrations Under Nonsteady Meteorological Conditions from Wind Tunnel Experiments," Journal of Applied Meteorology, Vol. 30, pp. 92-101.
- Li, W. W., Meroney, R. N., Peterka, J. A. (1981), "Wind-Tunnel Study of Gas Dispersion Near A Cubical Model Building," FDDL Report CER81-82WWL-RNM-JAP8, CSU, Fort Collins, Colorado, 97 pp.
- Lamb, R. G. (1982), "Diffusion in the Convective Boundary Layer," Chapter 5, Atmospheric Turbulence and Air Pollution Modeling, Nieuwstadt and van Dop, editors, D. Reidel Publishing Company, Dordrecht, Holland, pp. 159-230.
- Meroney, R. N. (1980), "Wind-Tunnel Simulations of the Flow Over Hills and Complex Terrain," J. of Industrial Aerodynamics, Vol. 5, pp. 297-321.
- Meroney, R. N. (1982), "Turbulent Diffusion Near Buildings," Engineering Meteorology, Chapter 11, pp. 481-521.
- Meroney, R. N. (1988), "Wind-Tunnel Modeling of the Flow About Bluff Bodies," J. of Wind Engineering and Industrial Aerodynamics, Vol. 29, pp. 203-223.
- Meroney, R. N., Cermak, J. E., Garrison, J. A. (1975a), "Wind-Tunnel Study of Stack Gas Dispersal at Lansing Power Station, Units 1, 2, 3, and 4," FDDL Report CER74-75RNM-JEC-JAG28, CSU, Fort Collins, Colorado.
- Meroney, R. N., Cermak, J. E., Garrison, J. A. (1975b), "Wind-Tunnel Study of Stack Gas Dispersal at Lansing Power Station, Units 1, 2, 3, and 4," FDDL Report CER74-75RNM-JEC-JAG29, CSU, Fort Collins, Colorado.
- Meroney, R. N., Tan, T. Z. (1990), "Wind-Tunnel Modeling of the Dispersion of Odorants and Toxic Fumes About Hospitals and Health Centers," 1990 EPA/A&WMA International Symposium on Measurement of Toxic and Related Air Pollutants, Raleigh, North Carolina, April 30-May 4, 1990.
- Neff, D. E., Tan T. Z., Meroney, R. N. (1988), "Fluid Modeling of Exhaust Gas Dispersion from the Boston-Edison Ventilation Site, Central Artery/Third Harbor Tunnel Project," FDDL Report CER88-89DEN-TZT-RNM-7, CSU, Fort Collins, Colorado, 65 pp.

- Neff, D. E., Tan T. Z., Meroney, R. N. (1988), "Fluid Modeling of Exhaust Gas Dispersion from the Parcel 7 Ventilation Site, Central Artery/Third Harbor Tunnel Project," FDDL Report CER88-DEN-RNM-6, CSU, Fort Collins, Colorado, 74 pp.
- Ogawa, Y., Diosey, P. G., Uehara, K., Ueda, H. (1985), "Wind Tunnel Observation of Flow and Diffusion Under Stable Stratification," *Atmos. Envir.*, Vol. 19, pp. 65-74.
- Peterka, J. A., Meroney, R. N., Kothari, K. (1985), "Wind Flow Patterns About Buildings," *J. of Wind Engineering and Industrial Aerodynamics*, Vol. 21, pp. 21-38.
- Plate, E. J., Cermak, J. E. (1963), "Micro-meteorological Wind-Tunnel Facility," FDDL Report CER63-EJP-JEC9, CSU, Fort Collins, Colorado, 65 pp.
- Poreh, M., Cermak, J. E. (1984), "Wind Tunnel Research on the Mechanics of Plumes in the Atmospheric Surface Layer, Part II," Annual Report to U.S. Dept. of Army, Chemical Systems Laboratory, Aberdeen Proving Ground, Maryland, FDDL Report CER84-85MP-JEC47, CSU, Fort Collins, Colorado, 45 pp.
- Fanga Raju, K. G., Singh, V. (1976), "Blockage Effects on Drag of Sharp Edged Bodies," *J. of Industrial Aerodynamics*, Vol. 1, pp. 301-309.
- Schlichting, H. (1968), Boundary Layer Theory, McGraw-Hill Book Company, New York, 774 pp.
- Schon, J. P., Mery, P. (1971), "A Preliminary Study of the Simulation of Neutral Atmospheric Boundary Layer Using Air Injection in a Wind Tunnel," *Atmos. Enviro.*, Vol. 5, No. 5, pp. 299-312.
- Seinfeld, J. H. (1986), Atmospheric Chemistry and Physics of Air Pollution, John Wiley & Sons, Inc., 738 pp.
- Simiu, E., Scanlan, R. H. (1986), Wind Effects on Structures, 2nd Ed., John Wiley & Sons, Inc., 589 pp.
- Snyder, W. H., Britter, R. E., Hunt, J. C. R. (1979), "A Fluid Modeling Study of the Flow Structure and Plume Impingement on a Three-Dimensional Hill in Stably Stratified Flow," Proceedings of the Fifth International Conference on Wind Engineering, Pergamon Press, NY, Vol. 1, pp. 319-329.
- Snyder, W. H. (1981), "Guidelines for Fluid Modeling of Atmospheric Diffusion," EPA Report EPA-600/8-81-009, 185 pp.
- Szechenyi, E. (1975), "Supercritical Reynolds Number Simulation for Two dimensional Flow over Circular Cylinders," *J. Fluid Mech.*, Vol. 70, pp. 529-542.
- Tan, T. Z., Meroney, R. N. (1989), "Fluid Modeling of Exhaust Gas Dispersion for the University of Colorado Health Sciences Center," FDDL Report CER88-89TZT-RNM-17, CSU, Fort Collins, Colorado, 54 pp.
- Teunissen, H. W. (1975), "Simulation of the Planetary Boundary Layer in a Multiple Jet Wind Tunnel," *Atmos. Envir.*, Vol. 9, pp. 145-174.
- Willis, G. E., Deardorff, J. W. (1974), "A Laboratory Model of the Unstable Planetary Boundary Layer," *J. Atmos. Sci.*, Vol. 31, pp. 1297-1307.
- Willis, G. E., Deardorff, J. W. (1976), "A Laboratory Model of Diffusion into the Convective Planetary Boundary Layer," *Quart. J. Roy. Meteorol. Soc.*, Vol. 102, pp. 427-445.
- Willis, G. E., Deardorff, J. W. (1978), "A Laboratory Study of Dispersion from an Elevated Source Within a Modeled Convective Planetary Boundary Layer," *Atmos. Envir.*, Vol. 12, pp. 1305-1311.
- Yamada, T., Meroney, R. N. (1971). "Numerical and Wind-Tunnel Simulation of Response of Stratified Shear Layers to Nonhomogeneous Surface Features," FDDL Report CER70-71TY-RNM62, CSU, Fort Collins, Colorado, also (AD-730-953).

Appendix: FLUID MODELING

The atmospheric boundary layer is that portion of the atmosphere extending from ground level to a height of approximately 1000 meters within which the major exchanges of mass, momentum, and heat occur. Since this is the region within which near-source diffusion occurs, it is the focus of the atmospheric modeling in this study. This section of the atmosphere is described mathematically by statements of conservation of mass, momentum and energy (Cermak, 1975). The mathematical requirements for rigid laboratory/atmospheric-flow similarity may be obtained by fractional analysis of these governing equations (Kline, 1965). This technique scales the pertinent variables by size and then transforms the equations into dimensionless form by dividing by one of the coefficients (in this case the inertial terms).

For similarity to exist between two flows not only must certain dimensionless parameters be equal for both systems, but there must also be similitude between the surface-boundary conditions and the approach flow wind field. Surface-boundary condition similarity requires equivalence of the following features:

- a. Surface-roughness distributions,
- b. Topographic relief, and
- c. Surface-temperature distribution.

If all the foregoing requirements are met simultaneously, all atmospheric scales of motion ranging from micro- to mesoscale could be simulated within the same flow field. However, existing laboratory facilities are not capable of simultaneously satisfying these restrictions; consequently a partial or approximate simulation must be used. This limitation requires that atmospheric simulation for plume dispersion must be designed to simulate most accurately those scales of motion which are of greatest significance for the transport and dispersion of plumes.

A.1 Dimensionless Parameters

Dimensional analysis is a technique that is used primarily for obtaining information about physical systems that are too complicated for full mathematical solutions to be feasible. Use of this tool enables (in part) the prediction of large systems from the study of small-scale models. By creating groups of quantities with zero overall dimensions modeling similarity is insured, provided that the *groups'* total value remains unchanged for both the model and prototype, while the value of

particular *quantities* (such as scale) may be changed. Dimensionless scaling parameters that are pertinent to this study are listed below.

Eckert number	$Ec = [U^2/C_p \Delta T]_r$	
Froude number	$Fr = [U^2/gL]$	= $\frac{\text{Inertial Force}}{\text{Gravitational Force}}$
Prandtl number	$Pr = [\nu/(k/\rho C_p)]_r$	= $\frac{\text{Viscous Diffusivity}}{\text{Thermal Diffusivity}}$
Reynolds number	$Re = (UL/\nu)_r$	= $\frac{\text{Inertial Force}}{\text{Viscous Force}}$
Richardson number	$Ri = [(Lg\Delta T/T)/U^2]_r$	= $\frac{\text{Gravitational Force}}{\text{Inertial Force}}$
Rossby number	$Ro = (U/L\Omega)_r$	= $\frac{\text{Inertial Force}}{\text{Coriolis Force}}$
Mach number	$Ma = [U/c]$	= $\frac{\text{Free stream velocity}}{\text{Velocity of sound}}$
Weber number	$We = [\rho U^2 L/\sigma]$	

For many fluid modeling situations several of the previously mentioned parameters are unnecessarily restrictive and may be relaxed without causing a significant loss in similarity between model and field fluid flow. The Rossby number magnitude controls the extent to which the mean wind direction changes with height. The effect of Coriolis-force-driven lateral wind shear on wind flow is only significant when heights are of the same order of magnitude as the boundary layer height. The Eckert number (in air $Ec = 0.4 Ma^2 (T_r/\Delta T_r)$, where Ma is the Mach number) is the ratio of energy dissipation to the convection of thermal energy. Both in the atmosphere and the laboratory flow, the wind velocities and temperature differences are such that the Eckert number is very small, and may be neglected. Prandtl number equality guarantees equivalent rates of momentum and heat transport. Since air is the working fluid in both the atmosphere and the laboratory, Prandtl number equality is always maintained. The approach flow Richardson number (Ri) and Reynolds number (Re) determine the kinematic and dynamic structure of turbulent flow within a boundary layer. This influence is apparent in the variations that occur in the spectral distribution of turbulent kinetic energies with changing Ri and changing Re . The effects of these two parameters are of considerable importance in this study and are discussed in the following sections.

A.1.1 The Reynolds Number

Re equality implies $U_m/U_p = L_p/L_m$. Re equality at a significantly reduced length scale would require that the model's flow velocity to be above sonic, which isn't very feasible for most conventional studies. Hence, Re equality must be distorted. A reduced Re changes only the higher frequency portion of an Euler-type description of the spectral energy distribution. Unfortunately, there is no precise definition as to which portion of an Euler Spectrum is dominant in dispersing ground-level or elevated plumes over moderate travel distances.

Most investigators use a minimum Reynolds number requirement based on rough-walled pipe measurements, (i.e., $Re = u_* z_o / \nu > 2.5$) where u_* , the friction velocity, and z_o , the roughness length, are derived from a log-linear fit to a measured mean velocity profile. The value 2.5 is an empirically determined constant. At Re below 2.5, it is observed that the mean velocity profiles in turbulent pipe flow lose similarity in shape and deviate from the universal curve of a rough wall turbulent boundary layer. For Re above 2.5, it is observed that the surface drag coefficient (and thus the normalized mean velocity profile) is invariant with respect to increasing Re. For Re between 0.11 and 2.5, the velocity profiles are characteristic of smooth wall turbulent boundary layers. For values below 0.11, the growth of a laminar sublayer on the wall is observed to increase with decreasing Re.

Extrapolation of results from pipe flow measurement to flat plate boundary layers may cause a shift in the magnitude of the minimum Re requirement, but it is generally felt that this shift is small. Precise similarity in the universal form of mean wind shear may be necessary for invariance with respect to the surface drag coefficient, but this does not necessitate that precise similarity must exist for the invariance of the wind field and dispersion. It is the distribution of turbulent velocities which has the greatest effect on the wind field and dispersion. However it is the mean wind shear which generates the turbulent velocities. It is possible that the specification of a minimum Re of 2.5 is overly conservative.

A.1.2 The Richardson Number

Although most wind-tunnel investigations are conducted with neutrally stratified boundary layers, there are circumstances when the stratification of the atmosphere must be considered. In particular, air pollution and dispersion problems are often critical during stratified conditions. Unstable stratification may be expected to mitigate hazards by accelerating plume dilution, whereas stable stratification may permit high concentrations to persist. The stability state of the atmosphere is typically characterized by the Richardson number.

The atmospheric gradient Richardson number can be computed from averaged quantities through the equation

$$Ri = g/T (\Gamma_d - \Gamma) [1 + 0.07/B] [(\partial u/\partial z)^2 + (\partial v/\partial z)^2]$$

where Γ and Γ_d are the actual and dry adiabatic potential temperature lapse rates, and $B = [C_p(T_2 - T_1)] / [(Z_2 - Z_1)(Q_2 - Q_1)]$ is the Bowen ratio of sensible to latent heat flux at the surface. The Ri number can be taken to represent the ratio of the relative importance of convective and mechanical turbulence. Negative Ri numbers of large value indicate strong convection and weak mechanical turbulence; zero Ri numbers imply purely mechanical turbulence. Positive Ri numbers less than some critical value, $Ri_{critical}$, suggest the presence of mechanical turbulence damped by the density-induced buoyancy forces; for larger positive Ri numbers, turbulence essentially disappears, since the stratification overpowers production by wind shear. The critical Richardson number has a value near 0.25.

A.2 Performance of Previous Fluid Modeling Experiments

To obtain a predictive model for a specific plume dispersion problem, one must quantify the pertinent physical variables and parameters into a logical expression that determines their inter-relationships. This task is achieved implicitly for processes occurring in the atmospheric boundary layer by the formulation of the equations of conservation of mass, momentum and energy. These equations with site and source conditions and associated constitutive relations are highly descriptive of the actual physical interrelationship of the various independent variables (space and time) and dependent variables (velocity, temperature, pressure, density, concentration, etc.).

These generalized conservation statements subject to the typical boundary conditions of atmospheric flow are too complex to be solved by present analytical or numerical techniques. It is also unlikely that one could create a physical model for which exact similarity exists for all the dependent variables over all the scales of motion present in the atmosphere. Thus, one must resort to various degrees of approximation to obtain a predictive model. At present, purely analytical or numerical solutions of boundary layer, wake, and plume dispersion are unavailable because of the classical problem of turbulent closure (Hinze, 1975). However, boundary layer wind tunnels are capable of physically modeling plume processes in the atmosphere provided certain restrictions are met, as was discussed previously.

It is expected that the gases being released from the exhaust stacks of the buildings modeled in this study will be at approximately ambient temperature and density; consequently the gas mixtures used to simulate the effluents were mixed to have neutral buoyancy relative to the air within the test environment. For this study the bulk of the gas being released was nitrogen at room temperature (specific gravity ≈ 1). Consequently the plume mass flux, momentum flux and volume flux become approximately equivalent ratios, and the plume Froude number is not a relevant parameter. The gas was mixed with a small amount of tracer, (smoke, methane, ethane or propane) to allow its subsequent movement to be charted.

A number of studies have been performed in the Colorado State University Fluid Dynamics and Diffusion Laboratory to establish the mechanics of interaction of structures within flow fields. Meroney et al. (1978) summarized experimental data available from field and laboratory studies for neutral airflow over hills, ridges, and escarpments. Wind-tunnel model measurements were performed to study the influence of topography profile, surface roughness and stratification on the suitability of various combinations of these variables. Detailed tables of velocity, turbulence intensity, pressure, spectra, etc., were prepared to guide numerical model design and experimental rule of thumb restrictions.

Local heating and cooling of the earth's surface is the driving mechanisms for sea-land breezes, and anabatic and catabiotic winds which may inhibit or enhance airflow over land. Early laboratory work includes simulations of urban heat islands by Yamada and Meroney (1971) and Sethuraman and Cermak (1973), simulation of flow and dispersion at shoreline sites by Meroney et al. (1975a), and simulation of dispersion effects of heat rejected from large industrial complexes by Meroney et al. (1975b).

Meroney (1980) compared three model-field investigations of flow over complex terrain, suggested performance envelopes for realizable modeling in complex terrain, and discussed recent laboratory studies which provide data for valley drainage flow situations. Not all of the model/field comparison experiments performed in the past were successful. Many early studies had model approach flow velocity exponents near zero, were modeled as neutral flows when strong stratification effects were observed in the field; or had modeled unrealistic boundary layer depths, integral scales, or turbulence intensities. Still, few studies claimed unreasonable correlation, (although some were strongly self-critical) and most accomplished their prestated limited objectives. It would appear that the simulation hypothesis developed in the last few years is appropriate for physical modeling of flow over complex terrain when appropriate care is taken to simulate the approach flow conditions and to maintain simulation parameters equal between model and prototype.

Arya and Plate (1969), Arya (1975) performed velocity, temperature, and turbulence measurements in the lowest 15 percent of a 70 cm deep boundary layer over a smooth surface, where conditions ranged from unstable to moderately stable ($-0.3 < z/L_{mo} < 0.3$). Free stream flow speeds varied from 3 to 9 m/s, and temperature differences were about 40°C across the boundary layer. Cermak, Shrivastava and Poreh (1983) reported mean velocity and turbulence measurements made for a variety of simulated atmospheric boundary layers over different surface roughness. Free stream flow speeds varied from 2.4 to 3.0 m/s and temperature differences were from 150°C to -80°C across the boundary layer. Poreh and Cermak (1984) reproduced unstable lapse conditions including mixed layers and elevated inversions. They reproduced the characteristics of convective boundary layer turbulence measured in the atmosphere.

Diffusion studies made by Chaudhry and Meroney (1973) in stable boundary layers investigated previously by Arya (1969) have shown agreement of experimental results with Lagrangian similarity theory. Horst (1979) tested Lagrangian similarity predictions of crosswind-integrated ground concentration against the Prairie Grass diffusion experiment (Barad, 1958) and an experiment at Idaho Falls (Islitzer and Dumbauld, 1963). He reported good agreement for all stabilities at distances x/z_0 out to $2 \cdot 10^5$. Poreh and Cermak (1984, 1985) released plumes in their modeled mixing layer. Their plumes exhibited the plume lofting typical of ground sources and the descent typical of elevated sources, predicted from water tank experiments by Willis and Deardorff (1974, 1976, 1978) and numerically by Lamb (1982).

Fluid Mechanics Laboratory Staff at the Ecole Centrale de Lyon have studied unstable wind-tunnel boundary layers and compared them with the atmospheric boundary layer (Schon and Mery, 1971). Flow speeds were typically 2 to 4 m/s and the floor temperature was maintained 50°C above ambient. Comparisons with the Kansas data (Haugen et al., 1971) were quite satisfactory, but longitudinal turbulence intensities exhibited a slight Reynolds number dependence, and spectral energy was too low in the high frequency portions of the spectra. The most unstable flow they studied had a Monin-Obukhov scale length of about 1 m at model scales, or 500 to 1000 m when scaled to the atmosphere.

A.3 Modeling of Bluff Bodies

The interaction of an approach wind field with bluff bodies or structures constructed on the earth's surface is broadly termed "Building Aerodynamics." In a review article on this subject, Meroney (1982) discusses the character of bluff body flow about rectangular buildings and cylindrical cooling towers. Defects in velocity profiles can easily persist from 10 to 15 building heights downwind. Field and laboratory measurements of plume dispersion about the Rancho Seco Nuclear Power Station in Sacramento, California, confirm that cooling tower wake effects persist for significant downwind distances under a variety of stratification conditions (Allwine, Meroney and Peterka, 1978; Kothari, Meroney and Bouwmeester, 1981).

A.3.1 Simulation Criteria

Often atmospheric turbulence may cause only weak effects compared to the turbulence generated by buildings, obstacles, and terrain. The magnitude of the disturbance depends upon: the incident flow turbulence scale and intensity, details of the obstacle shape and surface roughness, and size of the obstacle compared to the boundary layer depth. Geometrical scaling implies that the ratio of all building dimensions must be reduced by the same ratio.

Several questions should be considered when modeling flows which include surface obstacles:

- a. What size obstacles should be disregarded?
- b. What detail or roughness on an obstacle need be included?
- c. To what upwind distance should all obstacles be included?
- d. At what point does the size of a modeled obstacle become too big for the wind tunnel? (When do blockage effects significant become significant?)
- e. What is the effect on the flow field of mismatching obstacle and approach flow length scales?
- f. What is the minimum allowable model obstruction Reynolds number?

These considerations are discussed in the following sections.

A.3.2 Obstacle size & detail

Boundary layer studies of rough surfaces reveal that if protuberances are of a size k , such that $u_*k/\nu < 5$, they will have little effect on the flow in a turbulent boundary layer. Thus, assuming a laboratory wind speed of 1 m/s and a typical friction coefficient $C_f/2 = (u_*/u)^2 = 0.0025$, obstacles of size less than 2 mm would go unnoticed.

Another question that arises is "How much detail is required for the building or obstacle model? The answer is dependent upon the size of the detail compared to the plume, and to the dominant mixing eddy size. If the obstruction is large enough to modify the separated wake over the main obstacle, then it must be included. Often an equivalent surface roughness is adequate. Snyder (1981) concludes a generic surface roughness criterion might be $u_*k/\nu > 20$. For a 1 m/s laboratory flow this results in model roughness elements equal to about 6 mm. But since the exterior flow is usually highly turbulent, the body typically includes a highly unsteady wake, and the u_* value to be used should be that acting on the building surface, rather than that of the approach flow. Consequently even this roughness may be unnecessarily large.

A.3.3 Upstream Fetch Modeling

Suppose there is another building, tree line, fence, cooling tower, or obstacle some distance, s , upstream of a meteorological measurement location; is it necessary to include this obstacle in the wind-tunnel model? Hunt (1974) showed that the velocity deficit in the wakes of cubes and cylinders is given approximately by:

$$DU_{mx}/U(h) = A (s/h)^{-3/2}$$

downwind of the separation bubble, where DU_{mx} is the maximum mean velocity deficit created by the obstacle, h is the height of the obstacle, S is the distance downstream of the obstacle, and A is a constant dependent upon the obstacle shape, orientation, boundary layer thickness, etc. Typically, $A = 2.5$, but it may range from 1.5 to 5.0. If we desire that

the velocity at the spill site be within 3 percent of its undisturbed value, Snyder (1981) recommends that any upstream obstacle as high as $s/20$ be included upstream in the model of the spill site. If the obstacle's width is much greater than its height (for example, a fence or ridge), one should include it in the physical model if its height is greater than $s/100$.

A.3.4 Blockage Effects

Because of the influence of wind-tunnel walls on the behavior of the flow past models, it is desirable to use small models or big tunnels, or both. On the other hand, larger models are not only easier to work with, but they may be needed for similarity reasons to achieve large enough Reynolds numbers. It is possible to identify three different types of effects of wind-tunnel constraints. The first is the simple "solid blockage" effect which arises because the fluid stream is unable to expand laterally as it normally would in unconfined flow. The second effect, called "wake blockage", results because the accelerated flow between an obstacle and the tunnel walls continues to "pinch" the wake flow region and reduce its normal lateral rate of growth. The third effect is produced by the growth of boundary layers on the tunnel walls which produce "wall boundary interference." Tunnel blockage can cause separation and reattachment locations to vary, produce higher velocities, larger wake turbulence, and modify the dispersion patterns in the vicinity of obstructions.

The ratio of the cross-sectional area of a model obstacle to that of the tunnel is called the "blockage ratio", BR. Mass continuity produces an average velocity 'speed-up' of $S = BR/(1-BR)$. Although wind tunnels with adjustable ceilings can compensate to some extent by raising the roof over the blockage, this is not a perfect solution to the problem. Measurements on building and cooling tower models placed in different size wind-tunnel test sections reveal major changes in the character of pressure distributions, separation, and wake growth in the presence of flow restricted by wind-tunnel side walls (Farell et al., 1977).

Blockage corrections, which are conventionally applied in aeronautical tunnels, cannot usually be applied to the typical asymmetric model configuration placed against the wall of a meteorological wind tunnel (Ranga Raju and Singh, 1976). Conventional wisdom now suggests the "rule of thumb" that blockage ratios greater than five percent should be avoided.

A.3.5 Flow over Sharp-Edged Obstacles

A number of authors have discussed flow studies about simple cubical or rectangular sharp-edged obstacles. An extensive review about such flow fields and the subsequent character of diffusion near obstacles has been provided by Hosker (1984). Peterka, Meroney and Kothari (1985) describe typical flow deviations which result from the presence of a sharp-edged building.

Consider the main features of the flow around a sharp-edged building. Typically, when the approach flow is normal to the building face, the flow separates from the ground upwind of the building and produces a "horseshoe"-shaped vortex which wraps around the base of the building. The surface streamline reattaches on the front of the building, and fluid parcels move up and down the building's forward face. An elevated streamline flows over the obstacle, dips down behind, and stagnates on the surface at the end of the recirculating cavity immediately downwind of the building. Sometimes separation streamlines from the forward building edges reattach to the same face, yet in other cases the streamlines enter the downwind cavity and mingle with the other recirculating fluid. Air which enters the cavity departs through turbulent mixing across the dividing streamlines, mingles with downwind-pointing vortices and is ejected laterally out of the cavity, or leaves suddenly during an exhalation when the entire cavity appears to collapse and then reform.

When a building is oriented obliquely to the wind, flow over the front side walls does not separate, but strong recirculation occurs on the downwind faces. Flow over the roof often produces counter-rotating "delta-wing" vortices which increase mixing over the top and in the wake of the building. These vortices can cause reattachment of the flow in the middle of the roof and serious plume downwash in the near wake. Other features of the flow near the building include vertical vortices produced by the vertical corners of the building.

Golden (1961) measured the concentration patterns above the roof of model cubes in a wind tunnel. Two sizes of cubes were used to vary the Reynolds number from 1000 to 94,000. The concentration isopleths in the fluid above the cube roof showed only slight variations over the entire range of Reynolds numbers studied. The maximum concentration on the roof itself was found to vary strongly with Reynolds numbers less than 11,000, but to be invariant with Reynolds numbers between 11,000 and 94,000. Frequently, modelers quote Golden's experiments as justification for presuming dispersion invariance when obstacle Reynolds numbers exceed 11,000. However, Golden's "11,000 rule" is limited to the measurement of concentrations at only one point on the roof of smooth-walled cubes placed in a uniform approach flow of very low turbulent intensity. It is probably quite conservative because the shear and high turbulence in a simulated atmospheric boundary layer are likely to further reduce the critical Reynolds number. Indeed, Halitsky (1968) observed that for dispersion in the wake region, no change in isoconcentration isopleths from passive gas releases was found to occur for values of Reynolds number as low as 3300.

Flow around sharp-edged obstacles will remain kinematically similar at very low Reynolds numbers. Wake width variation will be minimal, and obstacle generated turbulence scales and intensity will only vary slowly as Reynolds number decreases. Gas clouds dispersing in this environment will remain similar at very low model speeds.

A.3.6 Flow over Rounded Obstacles

Flow around a smooth cylinder is Reynolds number dependent. This dependence reflects changes in the nature of the boundary layer that forms over the cylinder and its behavior in the vicinity of the flow separation. At low Reynolds numbers, the boundary layer is laminar, and separation occurs easily under the influence of even modest positive pressure gradients. At higher Reynolds numbers, the boundary layer becomes turbulent and flow separation is delayed; i.e., the flow can move farther along a curved surface without separation. At prototype scales, obstacles are large enough that only turbulent separation occurs. However, model flows are usually at such low Reynolds numbers that the local boundary layer growing over a curved surface would be laminar. Most modelers attempt the reproduction of full-scale similarity around curved surfaces by artificially roughening the model surface to force transition to turbulence in these laminar boundary layers. This can be done by providing the surface with special (or artificial) roughness elements, for example, sandpaper, thin wires, or grooves. The height of the roughness, k , should be such that $Uk/\nu > 400$ and $k/R < 0.01$, where U is the mean wind speed at obstacle height, and R is the characteristic obstacle radius of curvature. Szechenyi (1975) studied flows about rough circular cylinders and determined that as Reynolds number decreases, roughening the surface becomes less effective. Fage and Warsap (1929) considered the effect of increasing the surface roughness of cylinders on their drag coefficient. Eventually, even ridiculously large roughness is ineffective.

Niemann and Ruhwedel (1980) compared pressures and forces about a 1:333 scale model to a full-scale hyperbolic cooling tower shell. They roughened their model with vertical ribs of height 0.09 mm and width 0.77 mm, producing a roughness coefficient of $k/2R = 0.0006$ and roughness Reynolds number, $Re_k > 270$. They found meridional forces on the cooling tower model and prototype were similar. Model Reynolds numbers were between 4.5×10^5 and 6.0×10^5 , and this corresponding to $U_m > 45$ m/s. But again these speeds are much higher than is appropriate for current measurements.

Halitsky et al. (1963) examined dispersion about a smooth-model nuclear reactor containment building (a hemisphere fitted on a vertical cylinder) and found a critical Reynolds number greater than 79,000. (Yet this critical Reynolds number was for flow very close to the vessel wall. The behavior of concentration isopleths further downwind is likely to be less Reynolds number dependent.)

Although the details of fluid motions around rounded obstacles vary significantly with Reynolds number, the gross features of the flow do not change. Even small models at low wind speeds will produce horseshoe-shaped ground vortices, elevated pairs, and regular vortex shedding. If the internal boundary layer over the obstacle is laminar, then the wake region will be broader and less intense.

A.4 Modeling of Plume Motion

In addition to modeling the turbulent structure of the atmosphere in the vicinity of a test site it is necessary to properly scale the plume source conditions. One approach would be to follow the methodology described earlier would be to write the conservation statements for the combined flow system followed by fractional analysis to find the governing parameters. An alternative approach, the one which will be used here, is that of similitude (Kline, 1965). The method of similitude obtains scaling parameters by reasoning that the mass ratios, force ratios, energy ratios, and property ratios should be equal for both model and prototype. When one considers the dynamics of gaseous plume behavior the following nondimensional parameters of importance are identified.¹

Mass Flux Ratio	=	$\frac{\text{mass flow of plume}}{\text{effective mass flow of air}}$
Momentum Flux Ratio	=	$\frac{\text{inertia of plume}}{\text{effective inertia of air}}$
Densimetric Froude Number (relative to the inertia of the air)	=	$\frac{\text{effective inertia of air}}{\text{buoyancy of plume}}$
Densimetric Froude Number (relative to the inertia of the plume)	=	$\frac{\text{inertia of plume}}{\text{buoyancy of plume}}$
Flux Froude Number	=	$\frac{\text{momentum flux of air}}{\text{buoyancy momentum flux of plume}}$
Volume Flux Ratio	=	$\frac{\text{volume flow of plume}}{\text{effective volume flow of air}}$

It is necessary to maintain equality of the plume's specific gravity, ρ_g/ρ_a , over the plume's entire lifetime to obtain simultaneous simulation of all of these parameters. Unfortunately a requirement for equality of the plume gas specific gravity for plume with significant buoyancy differences (i.e. ρ_g not equal ρ_a) leads to several complications in practice. These are:

- 1) Equality of the source gas specific gravity between a model and its atmospheric equivalent leads to a wind speed scaling from $(U_m/U_p)^2 = L_m/L_p$. For a significant range of atmospheric wind speeds this relationship leads to wind-tunnel speeds at which there is a possible loss of the Reynolds number invariance in the approach flow.

¹ The scaling of plume Reynolds number is also a significant parameter. Its effects are invariant over a large range. This makes it possible to accurately model its influence by maintaining model tests above a minimum plume Reynolds number requirement.

- 2) A thermal plume in the atmosphere is frequently simulated in the laboratory by an isothermal plume formed from a gas of appropriate molecular weight. Under certain situations of specific heat capacity mismatch, this practice will lead to a variation of the equality of plume density as the plume mixes with air.

It is important to examine each modeling situation and decide if an approximation to complete plume behavior may be employed without a significant loss in the similarity of the modeled plume structure.